

Hubble Space Telescope Snapshot Survey for Resolved Companions of Galactic Cepheids: Final Results ^{*†}

NANCY REMAGE EVANS,¹ H. MORITZ GÜNTHER,² HOWARD E. BOND,^{3,4} GAIL H. SCHAEFER,⁵ BRIAN D. MASON,⁶
MARGARITA KAROVSKA,¹ EVAN TINGLE,¹ SCOTT WOLK,¹ SCOTT ENGLE,⁷ EDWARD GUINAN,⁷ IGNAZIO PILLITTERI,⁸
CHARLES PROFFITT,⁴ PIERRE KERVELLA,⁹ ALEXANDRE GALLENNÉ,^{10,11,12} RICHARD I. ANDERSON,¹³ AND MAXWELL MOE¹⁴

¹*Smithsonian Astrophysical Observatory, MS 4, 60 Garden St., Cambridge, MA 02138; nevans@cfa.harvard.edu*

²*Massachusetts Institute of Technology, Kavli Institute for Astrophysics and Space Research, 77 Massachusetts Ave, NE83-569, Cambridge MA 02139, USA*

³*Department of Astronomy and Astrophysics, Pennsylvania State University, University Park, PA, 16802*

⁴*Space Telescope Science Institute, 3700 San Martin Drive, Baltimore, MD 21218*

⁵*The CHARA Array, Georgia State University, P.O. Box 3965, Atlanta GA 30302-3965*

⁶*US Naval Observatory, 3450 Massachusetts Ave., NW, Washington, D.C. 20392-5420*

⁷*Department of Astronomy and Astrophysics, Villanova University, 800 Lancaster Ave., Villanova, PA, 19085, USA*

⁸*INAF-Osservatorio di Palermo, Piazza del Parlamento 1, I-90134 Palermo, Italy*

⁹*LESIA, Observatoire de Paris, Université PSL, CNRS, Sorbonne Université, Université de Paris, 5 Place Jules Janssen, 92195 Meudon, France*

¹⁰*Nicolaus Copernicus Astronomical Centre, Polish Academy of Sciences, Bartycka 18, 00-716 Warszawa, Poland*

¹¹*Departamento de Astronomía, Universidad de Concepción, Casilla 160-C, Concepción, Chile*

¹²*Unidad Mixta Internacional Franco-Chilena de Astronomía (CNRS UMI 3386), Departamento de Astronomía, Universidad de Chile, Camino El Observatorio 1515, Las Condes, Santiago, Chile*

¹³*European Southern Observatory, Karl-Schwarzschild-Str 2, 85748 Garching, Germany*

¹⁴*University of Arizona, Steward Observatory, 933 N. Cherry Ave., Tucson, AZ 85721, USA*

ABSTRACT

Cepheids in multiple systems provide information on the outcome of the formation of massive stars. They can also lead to exotic end-stage objects. This study concludes our survey of 70 galactic Cepheids using the *Hubble Space Telescope* (*HST*) Wide Field Camera 3 (WFC3) with images at two wavelengths to identify companions closer than 5". In the entire WFC3 survey we identify 16 probable companions for 13 Cepheids. The seven Cepheids having resolved candidate companions within 2" all have the surprising property of themselves being spectroscopic binaries (as compared with a 29% incidence of spectroscopic binaries in the general Cepheid population). That is a strong suggestion that an inner binary is linked to the scenario of a third companion within a few hundred AU. This characteristic is continued for more widely separated companions. Under a model where the outer companion is formed first, it is unlikely that it can anticipate a subsequent inner binary. Rather it is more likely that a triple system has undergone dynamical interaction, resulting in one star moving outward to its current location. *Chandra* and *Gaia* data as well as radial velocities and *HST*/STIS and *IUE* spectra are used to derive properties of the components of the Cepheid systems. The colors of the companion candidates show a change in distribution at approximately 2000 AU separations, from a range including both hot and cool colors for closer companions, to only low-mass companions for wider separations.

Keywords: stars: binaries; stars: intermediate mass; stars: Cepheid variable; star formation: multiple star systems

1. INTRODUCTION

Binary and multiple systems are very common products of star formation. This is increasingly so for more massive stars. Properties such as separation, mass ratio, and eccentricity are the “footprints” of star formation, providing observational insight into the process. Separations between components of the systems determine which observational

* Based on observations with the NASA/ESA *Hubble Space Telescope*, obtained at the Space Telescope Science Institute, which is operated by the Association of Universities for Research in Astronomy, Inc., under NASA contract NASA5-26555.

† Based on observations made with the *Chandra X-ray Observatory*

approaches can be used to study them, as summarized by Figure 1 in Sana (2017). These include radial velocities for close binaries and many new techniques for resolving more distant companions. Duchêne & Krauss (2013) provide a recent summary of observations of multiple systems. Evolution of systems can occur at the pre-main sequence phase, or post-main-sequence phase through Roche-lobe overflow and dynamical interaction. Formation and evolution of massive stars in multiple systems is particularly complex (de Mink et al. 2014), and a high fraction of O stars undergo interaction and mergers. The formation scenario in multiple systems probably involves core fragmentation, leading to relatively wide separations followed by disk fragmentation for closer components and subsequent migration for very close components. Complex multiple systems, however, can be produced by more than one scenario (Tokovinin 2018a).

The formation of wide binaries presents a puzzle. The most likely scenarios are the unfolding of triple systems (Reipurth & Mikkola 2012), the dissolution of clusters (Kroupa 1995), and formation from adjacent cores (Tokovinin 2017).

As we are increasingly realizing, O and B stars often occur in systems with more than two stars, inevitably making the discussion of individual systems somewhat complicated. Cepheids (former B stars with typical masses of $5 M_{\odot}$) fall in the lower part of the mass range of O and B stars. However there are several features of Cepheid systems which mean they make an important contribution to an accurate picture of the distribution of masses and separations in multiple systems. They are a well-defined sample of evolved helium-burning stars. They are less rare than O stars, providing more examples which can be resolved by interferometric techniques. The combination of a cool evolved star and a hot companion leads to uncontaminated spectra of both the brightest and hottest stars in the system at different wavelengths. Finally, Cepheid parameters are easier to relate to their main-sequence B-star counterparts than more massive stars, since mass loss on the main sequence is minimal. However, formation and the main-sequence stages for Cepheids are not the end of the story. From B-star binary statistics we know that approximately a third of Cepheids are the products of mergers (Moe & Di Stefano 2017; Sana et al. 2012). This is a good example, however, of a complication which we have information to understand, since it will have only affected short-period main-sequence binaries. In addition to understanding how multiple systems are formed (and what they tell us about the process), multiple systems, especially those containing massive stars, are important in many exotic end stage objects. They are implicated in creating many objects such as X-ray binaries, millisecond pulsars, supernovae, Algols, and perhaps gamma-ray bursts and gravitational radiation sources. Moe & Di Stefano (2017) review binary properties involved in such outcomes.

The current study is part of a series aimed at determining the binary/multiple properties of Cepheids. The first paper (Paper I; Evans et al. 2013) is a discussion of the binary properties of a group of Cepheids with mass ratios greater than 0.4, compiled from a list observed by the *International Ultraviolet Explorer* (IUE) satellite. This list is equally sensitive to companions at any separation, making the distribution of separations unbiased. The second paper discusses a sample of 70 Cepheids observed with the *Hubble Space Telescope* (HST) Wide Field Camera 3 (WFC3) in two filters (Paper II; Evans et al. 2016a). This paper discusses candidate companions more distant than $5''$, where photometry of possible companions is not contaminated by the much brighter Cepheid. The current paper (Paper III) follows with a discussion of possible companions closer to the Cepheid. These studies are supplemented with a discussion of *XMM-Newton* X-ray observations of systems with possible companions, in order to determine whether the companion is young and active enough to be a physical companion of the Cepheid (Paper IV; Evans et al. 2016b). The study of resolved companions is complemented by a discussion of radial velocities for northern Cepheids (Evans et al. 2015).

The sections below discuss the observations and data reduction, both for Cepheids with companions separated between $2''$ and $5''$, and also companions within $2''$. *Chandra* X-ray observations are then used to verify companions. The discussion section summarizes candidate companions at all separations. Special attention is given to companions within $2''$, and the components of these complex systems are discussed in detail. This includes the color-magnitude diagram (CMD), the distribution of colors as a function of separation, and inner binaries of this group. Astrometric data from *Gaia* are used to identify wider companions, both gravitationally bound companions and comoving but unbound companions.

2. OBSERVATIONS AND DATA REDUCTION

Observations were made in our *HST* Wide Field Camera 3 (WFC3) snapshot program, which imaged 70 of the brightest Cepheids. The F621M and F845M filters were used; these can be transformed into the *V* and *I* bandpasses of ground-based photometry. (Throughout this paper all magnitudes discussed are on the Johnson-Kron-Cousins

Table 1. Candidate Cepheid Companions at Separations Between $2''$ and $5''$

F621M	F621M–F845M	V	$V - I$	Sep.	P.A.	Sep.
[mag]	[mag]	[mag]	[mag]	[arcsec]	[$^{\circ}$]	[AU]
Y Car						
16.45 ± 0.02	0.60 ± 0.02	16.91	0.93	2.6	55	3,820
16.79 ± 0.03	0.86 ± 0.03	17.40	1.29	3.2	112	4,700
V496 Aql						
18.39 ± 0.09	1.56 ± 0.09	19.05	1.99	4.3	78	4,250
TT Aql						
17.16 ± 0.05	1.40 ± 0.05	17.82	1.85	3.8	67	3,520
V350 Sgr						
17.24 ± 0.04	1.31 ± 0.04	17.91	1.77	3.1	128	2,780
BB Sgr						
17.41 ± 0.06	1.31 ± 0.07	18.08	1.77	3.3	158	2,740
RV Sco						
15.37 ± 0.01	0.90 ± 0.01	16.00	1.34	3.6	173	2,710

system.) Observations were made in a dithered sequence. The survey is described in Paper II, including the target list. The aim was to identify possible companions of the Cepheids, which are typically many magnitudes fainter. Because the point-spread function (PSF), dominated by the bright Cepheid, is complex, our data analysis has been divided into three sections, according to the angular distance from the Cepheid. For the area $\geq 5''$ from the Cepheid, the background is modest and only changes slowly, and hence photometry is straightforward to derive using standard tasks in IRAF.¹ The results for this separation range are discussed in Paper II.

In the current paper, we only treat the region within $5''$ of the central Cepheid. We subdivide this inner region again into two zones. Between $2''$ and $5''$, we again perform simple photometry with standard IRAF tasks (Section 3). The innermost regions are dominated by the bright Cepheid, where its extended PSF makes it challenging to perform source detection and measure photometry. In Section 4 we describe this in detail.

3. COMPANIONS BETWEEN $2''$ AND $5''$

Source detection and photometry between $2''$ and $5''$ separation from the Cepheid was done in the same way as for the more distant companions; details are provided in Paper II.

Once the list of sources between $2''$ and $5''$ had been generated, we tested them for the appropriate combination of magnitude and color for main-sequence stars at the distance of the Cepheid, as in Paper II. For the main-sequence relation, we used the Dartmouth Stellar Evolution Database² to generate an isochrone for a 1 Gyr age, for the pair of WFC3 filters we used, i.e., F621M absolute magnitude versus F621M–F845M color. Although this age—the minimum contained in the Dartmouth database (at the time of Paper II)—is older than that of the Cepheids (typically 50 Myr), even most deviant stars in this study (the late-K spectral-type stars) are only ~ 0.1 mag above this representation of the zero-age main sequence (ZAMS). To compare this ZAMS with the observed WFC3 photometry, we have “reddened” the color and “absorbed” the magnitude and “moved” it to the distance of the Cepheid. Full details (including the distances of the Cepheids) are provided in Paper II.

To select candidate companions of the Cepheids, we required them to lie within 2σ of a band lying between the ZAMS and a parallel line 0.75 mag above it (to allow for binaries). These candidates are listed in Table 1. Appendix A contains Figures 10 to 15, which illustrate the WFC3 images for the candidates in Table 1, and plot the CMDs for each field. The present paper focuses on possible companions within $5''$; consequently there are some additional stars

¹ IRAF was distributed by the National Optical Astronomy Observatories, operated by the Association of Universities for Research in Astronomy, Inc., under cooperative agreement with the National Science Foundation.

² <http://stellar.dartmouth.edu/models/index.html>

within the ZAMS band which lie at larger separations from the Cepheid; these were discussed in the previous paper (Paper II).

Photometry of the candidate companions is listed in Table 1. The instrumental magnitudes have similar errors to those of more distant companions in the previous study derived from the statistics. However, we expect that there is some additional uncertainty due to a more variable background. Table 1 lists the instrumental F621M magnitude (F621M) and color (F621M–F854M) (columns 1 and 2). For convenience, these magnitudes have been transformed to ground-based V and $V - I$, using the relations in Paper II (Vegamags), and are given in columns 3 and 4. The separation in arcsec, the position angle, and the projected separation in AU (using the distances to the Cepheids from Paper II) are listed in columns 5, 6, and 7. (For V496 Aql, the position angle has been corrected in Table 1, from that in Table 5 in Paper II.)

4. COMPANIONS WITHIN $2''$

4.1. Data Reduction

For these close companions lying within the PSF wings of the bright Cepheid primaries, we proceeded as follows. The data processing started with the geometrically distorted, flat-fielded individual frames (FLT images) from the *HST* archive. We then applied a custom data-reduction procedure to deal with saturation and charge bleed.

4.1.1. Masking the Charge Bleed

The Cepheids are severely overexposed in our frames. Not only are the central pixels saturated, but the additional charge collected beyond saturation bleeds out to adjacent pixels. This happens predominantly along the columns of the CCD. In the vicinity of the Cepheid, pixels “bled into” also reach the saturation charge limit, and are flagged by the pipeline appropriately. However, we find that charge continues to bleed upwards and downwards along the columns, leading to severely enhanced charge levels up to two pixels beyond the fully saturated region. In addition, charge bleeds to the right (increasing x value in image coordinates) into the neighboring column. We thus add custom filtering to any pixel that is found to the right or one or two pixels above or below a pixel that is already marked as saturated by the standard pipeline. Gilliland et al. (2010) performed a similar analysis, and suggested increasing the region masked due to saturation by one pixel in any direction. In our data, on the one hand, that recipe leads to spurious enhanced emission above and below the bleed region where charge bleeds more than one pixel beyond the fully saturated region. On the other hand it masks out area to the left of the saturated regions that seems usable.

4.1.2. Combining Exposures

We combined individual exposures for each filter and each object using *astrodrizzle* from DrizzlePac (Hack et al. 2013). This algorithm projects the values of all contributing exposures onto the sky, and then, for every sky position, averages over all valid (non-masked) values. Since the individual exposures have slightly different boresight coordinates, pixels fall onto the sky differently. Thus, this procedure results in a smaller area masked due to bleed than in the individual images. On the other hand, close to the Cepheid, only one of three exposures might contribute valid data, while all three images are averaged at larger distances. Since the signal close to the Cepheid is high, the noise in the combined image is still acceptable. We chose $0''.0396$ as the pixel size in the resampled images.

4.1.3. Cutting Out Sub-images

In this section, we concentrate on close companions within $2''$. Because the Cepheids are all well saturated, we cannot determine the position of peak flux. Instead, we fit straight lines to the diffraction spikes (diagonals in our images) and take the intersection of the diffraction spikes as the position of the Cepheid. We then extract sub-images 120 pixels on each side, centered on the Cepheid. Based on the uncertainties of the fit to the diffraction spikes, we estimate that this procedure is accurate to about one pixel.

4.2. PSF Subtraction and Fitting

Sources more than $2''$ from the Cepheid are discussed in Paper II and Section 3 above. In this section, we study the region within $2''$, where the image is dominated by the PSF of the Cepheid.

4.2.1. Locally optimized combination of images (LOCI)

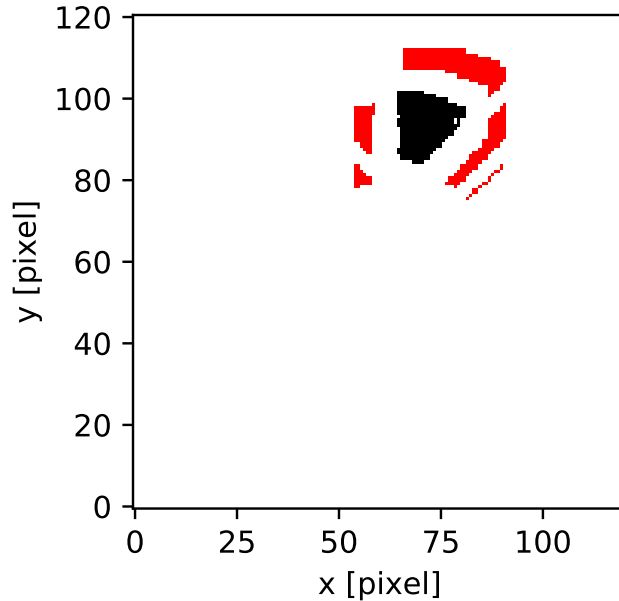


Figure 1. Example of an optimization region in LOCI. To find the best possible combination of the PSF templates for the black region, we actually fit in the red region. This way, a moderately bright point source in the black region does not impact the results of the fit. Note how the red region does not completely envelop the black region, but has gaps avoiding regions that are contaminated by bleed or diffraction spikes or where one of the reference images cannot be used because it has a candidate companion itself.

In order to detect and perform photometry on potential companions, we need to subtract the PSF of the Cepheid itself. This is challenging since the *HST* PSF changes with time. Several observational and computational approaches to detect faint sources close to a much brighter primary have been developed in the past years, especially with an application to exoplanets. One of the most common observational techniques is angular differential imaging, where the same source is observed more than once with a different orientation of the instrument, such that instrumental features rotate on the sky, but true companions are fixed in sky coordinates. The scheduling of a snapshot program did not allow for this approach, so we are limited to computational methods to reduce the impact of the Cepheid PSF. Lafrenière et al. (2007) introduced a method called “locally optimized combination of images” (LOCI); see their paper for a mathematical description of the algorithm. In short, this algorithm describes an image as a linear combination of companion-free reference images. The coefficients that lead to the smallest residual between target image and the combination of reference images can be found essentially by a matrix inversion, which is computationally more efficient than numerical function minimizers. Fitting the whole image at once would introduce two major problems. First, the temporal change in the PSF might depend on the position, e.g., some parts of the PSF change more than others due to a temperature change of the telescope. Describing the full image at once thus requires a large number of reference images. Second, if a companion exists and is included in the fit, the fit will try to subtract it as much as possible, compromising the photometry. Thus, for LOCI the image is divided into several smaller regions. To find the best linear combination of templates for a specific region, we perform the optimization on an area that is *outside* the region of interest (see Figure 1).

4.2.2. Modification of standard LOCI procedures

Several enhancements of the LOCI method developed by Lafrenière et al. have been suggested in the literature, including “template LOCI” (Marois et al. 2014), which considers spectral information, or “matched LOCI” (Wahhaj et al. 2015), which inserts artificial point sources with known properties to inform the fitting process. Another approach is to decompose the set of PSF templates into eigenimages, thus using information from all images to isolate the true PSF components and separate them from observational noise that varies from image to image (Soummer et al. 2012). After reviewing these ideas in the literature, we modified the basic LOCI algorithm for the specific characteristics of our dataset.

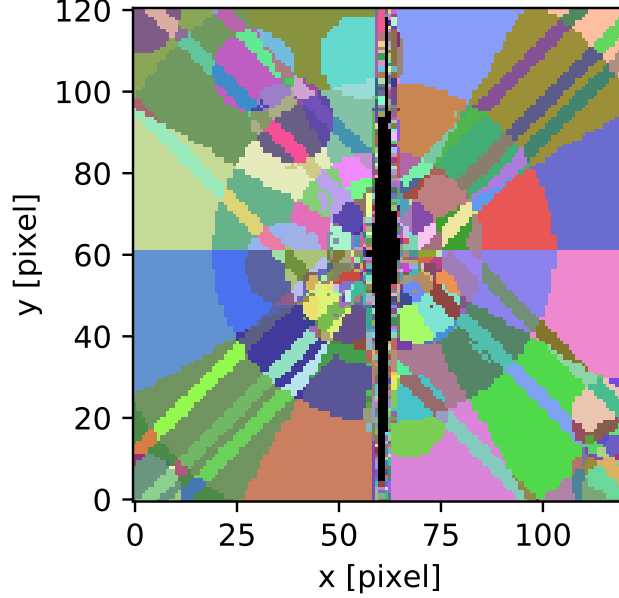


Figure 2. An image is typically divided into more than 500 regions for fitting. Each color shows one region. Apparent circle shapes (e.g., the circle centered on (55, 110)) are due to potential companions in one of the images, forcing a smaller set of templates in that region. Similarly, diagonal lines are due to diffraction spikes from bright companions that we masked.

For any one Cepheid observation, we use the set of the other 69 observations taken in the same filter in our program as template images. This is justified because they are all taken within a few months of each other, use an identical instrumental setup (except for the exposure time), and all expose the central source well into saturation, bringing out faint PSF features visible beyond $2''$, which are generally hidden in the noise for other archival data taken in the same filter. The drawback of this method is that some of the template images might themselves contain companions, which would leave negative imprints in the reduced images. We thus perform an initial source detection (see next subsection) and mask regions potentially affected by a companion. For fits involving this region, only the remaining 68 images are used as templates. Similarly, the region affected by bleed differs from image to image. To perform a fit close to the central source, we used only those images that have valid data in this region as fitting templates. Following this prescription, a typical image in our dataset is separated into more than 500 regions, each potentially with a different set of template images (Figure 2).

4.2.3. Initial source detection

The very brightest companions (see Table 2) are themselves saturated and are easily visible by eye. To identify other companions we need to mask before using images as LOCI templates, we construct a median image. The magnitude of the Cepheids is very different and this is not fully compensated by choosing different exposure times. The flux level in the images differs by about a factor of 1000 between the brightest and faintest image. We normalize each image by dividing the image by its median value. As a second step, we form a median image from all normalized images for each band. The median images show the shape of the average PSF, not including any companions. We then divide each normalized image by the median image. The result of this is an image that shows how each dataset deviates from the median PSF. While not flux-conserving, this procedure works well to highlight potential companions. We use the `daofind` algorithm from Stetson (1987) as implemented in `photutils` to locate potential point sources and mask those before performing LOCI fitting. At this stage we identify 17 potential companions and mask their positions in both filters. Not all of those sources will turn out to be real, but we can be conservative here because masking a potential source just means that only one image cannot be used as PSF template in one region (see Figure 2 for an example), which has little impact on the quality of the fit given that the set of potential templates consists of 69 images.

4.2.4. Application of LOCI and PSF fitting

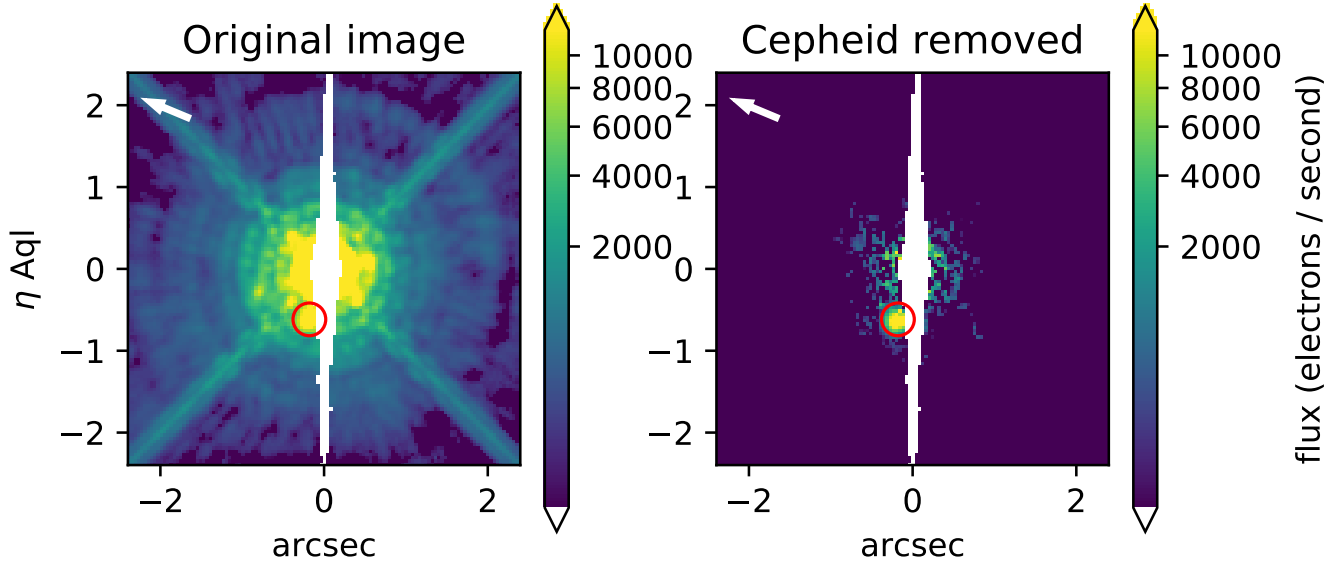


Figure 3. Image of η Aql in the F845M band. Several bright PSF features are seen within $1''$ of the Cepheid position. The image is oriented along the detector coordinates. The white arrow points north. *Right:* The companion is clearly visible after the LOCI subtraction.

We perform LOCI fitting to each of our images and subtract the result of the best fit in each region from the original image. Figure 3 shows an example. Most of the PSF features, including the diffraction spikes, are significantly reduced, but within about $1''$ from the Cepheid, residuals from the subtraction increase. We find that source-detection algorithms do not perform well in this region. We thus inspect every image by eye and perform PSF photometry on all source candidates from §4.2.3. In principle, our procedure requires iteration, where any new sources identified would now be masked and the LOCI fitting repeated. However, no new sources beyond the previous candidates are identified. Table 2 lists the resulting source detections.

4.2.5. Uncertainty estimates

The uncertainty of the properties of the companion is dominated by systematics introduced through the LOCI subtraction. Additionally, there is a risk of oversubtraction in the LOCI procedure. We quantify those effects through simulations where we insert fake sources with known fluxes into the images, run the same LOCI subtraction and measure the flux of the detected companions. From our images, we select sources not visibly impacted by the PSF of the Cepheid. We checked the *Gaia* Data Release 2 (DR2) catalog (Gaia Collaboration et al. 2016, 2018) for these sources. While this release does not explicitly mark extended or multiple sources, the errors on the coordinates are a good proxy. We reject any sources with *Gaia* coordinate errors above 0.1 milliarcsec as likely binaries. We fit a beta function as analytical PSF to the remaining sources and reject sources where fitted parameters are significantly different than the sample mean. We end up with a set of 18 PSF template stars. We fix the parameters of the shape and use the resulting analytical PSF for fits to both the real data (§4.2.4) and the LOCI subtracted images with fake companions inserted.

For each template star, we extract squares 25 pixels wide, centered on those sources, from background-subtracted images. For each simulation, we select one of those sources, scale its F621M and F845M flux as required and add it to one of the original Cepheid images. We then perform LOCI subtraction on the image with the artificially inserted companion and measure the source flux through PSF photometry. For each source in Table 2 we run 200 simulations. Depending on the position of the companion in Table 2, we select positions similarly effected by the Cepheid PSF. For instance, for R Cru, where the companion is found almost $2''$ from the Cepheid, but only a few pixels from the bleed column, we inject the artificial companions into the image on the opposite side of the Cepheid with a similar distance to the bleed column (Figure 4) and vary the insert location slightly to probe any background fluctuations statistically. Typically, some of the companion flux is subtracted in the LOCI procedure and thus the measured magnitudes (pink

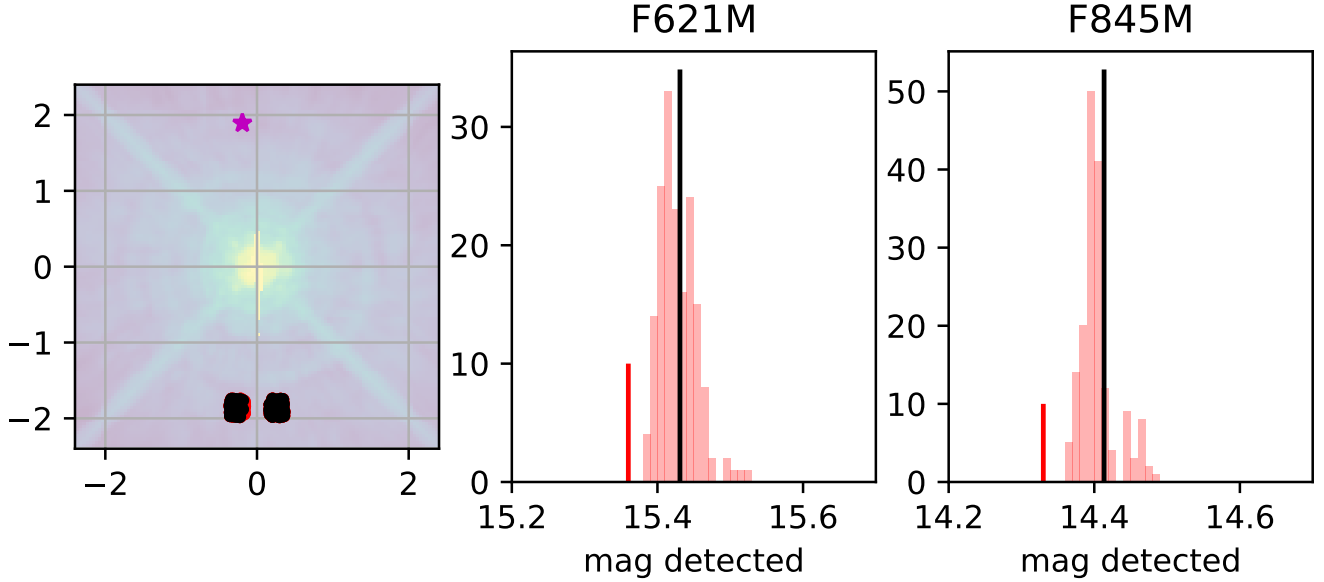


Figure 4. *left:* Image of R Cru in the F621M band. The image is oriented along the detector coordinates. The purple star marks the location of the detected companion. Fake companions are inserted at a location where the PSF of the Cepheid is comparable, here below the Cepheid at a similar distance to Cepheid and bleed column. Black dots are inserted companions that are recovered by the fit procedure, red dots are companions not recovered (e.g. because they are located too close to the bleed column). *center and right:* Histogram of the recovered magnitudes of inserted companions for each filter. The red line marks the true magnitude of the inserted companions; the black line measured magnitude of the companion in the real image.

histograms in Figure 4) are fainter than the input magnitudes (red line). We thus conclude that the true flux of the companion in the real image must also be higher than the measured flux and we apply the offset determined from the simulations to correct the measured companion magnitude (black line). We take the standard deviation of the simulated magnitudes as the error estimate for the companion flux because the distribution of magnitudes is typically peaked, but the distribution has a significant tail towards fainter magnitudes for S Nor, which means the true magnitudes could be up to 0.5 mag brighter than the number given in Table 2.

4.2.6. Saturated companions

This procedure cannot be applied for the very brightest companions that are themselves saturated, because we do not have PSF template stars of comparable brightness. If the companion’s core is saturated, PSF photometry can in principle determine the flux by fitting the wings of the PSF. However, our template stars are not bright enough to determine the shape of the wings accurately enough. Similarly, the template stars would have to be scaled up significantly to be inserted into images for our simulations that determine the flux uncertainties, but this would significantly enhance the noise. However, for a measurement of the position alone, the exact shape of the PSF wings is not important and we thus provide positions for the saturated companions in Table 2.

4.3. Results

4.3.1. Completeness

To quantify our detection limits, we employ a procedure similar to our uncertainty estimate for detected companions. We insert companions into Cepheid images at a certain radius from the Cepheid, apply our source-detection algorithm, and measure the fraction of companions recovered in both bands. The inserted companions have a color $m_{621} - m_{845} = 1$, similar to the values observed in the detected companions (Table 2). We verified that the detection fraction changes little for reasonable choices of this color. Figure 5 shows the limits. We note that these limits describe the detectability in our whole sample. The flux level at a given distance from the Cepheid differs by three orders of magnitude between the brightest and faintest image due to different exposure times and Cepheid magnitudes and thus a companion that

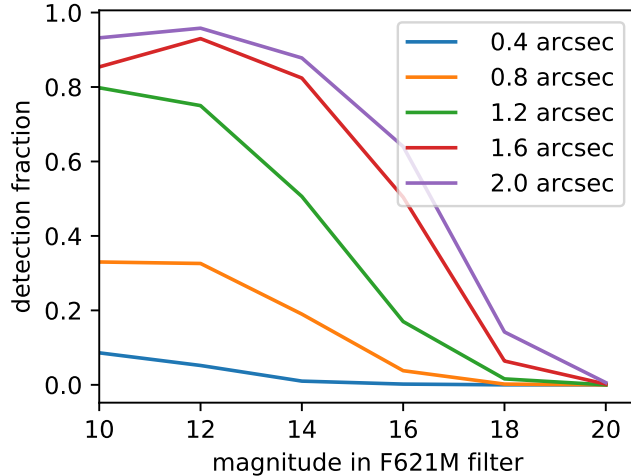


Figure 5. Detection fraction for companions depending on distance from the Cepheid and flux from the companion.

could be detected in one image, can be hidden in the background in another. We note further (in the image segments we discuss outside of $0''.5$) that between $1''$ and $0''.5$ the bleed column obliterates a significant part of the image.

At $0''.4$, only a small fraction of companions is detected, even for the brightest sources. For bright sources, this number rises quickly with increasing distance and beyond $1''$, most companions with $m < 12$ that do not overlap the diffraction spikes or the bleed columns are detected. Fainter companions require larger distances. Only for distances beyond $1''$ are more than half of the $m_{621} = 16$ companions detected.

4.3.2. Detected companions

The images in which companion candidates were detected are shown in Figure 3, and Figures 16 to 24 in Appendix B, both before and after PSF correction.

Table 2 lists the detected companions. It gives both the raw, measured magnitude and the corrected magnitude based on the simulations. The uncertainty given is also taken from the simulations. No correction can be derived for the brightest three companions (around η Aql, V659 Cen, and AX Cir), because those companions are themselves saturated. Fluxes are highly uncertain, but separation and position angle only rely on the assumption that the PSF is rotationally symmetric. The uncertainties in the position angle, like the uncertainties in the fluxes, are dominated by residuals from the LOCI procedure. We analyze fake inserted sources and find that essentially all inserted sources are recovered within 5 pixels ($0''.2$) of the inserted position, while the large majority of sources are found within half that distance. These are upper limits to the positional uncertainty for true companions, because our insertion procedure can add sources only at integer-valued positions, introducing an additional shift up to half a pixel.

The photometry in Table 2 has been converted to V and I in the same way as in Paper II, using the corrected photometry. The results are listed in Table 3. Distance and reddening are also from Paper II, with the distance based on the Benedict et al. (2007) Leavitt Law. The separation in AU is also listed, based on this distance.

The LOCI search also identified three additional sources in the postage stamps, which are listed in the last three rows of Table 2 and Table 3. In the case of BG Cru, the source lies on a diffraction spike, and required LOCI processing to identify it. V and $V - I$ for CO Aur are based on uncorrected magnitudes in Table 3. However, if we use the distance to the Cepheid, all three companions are too faint to be consistent with a ZAMS relation. For BG Cru, for instance, the $(V - I)_0$ corresponds to an F8 V star (Drilling & Landolt 2000), which would have $M_V = +4.0$. The V , $E(B - V)$, and distance, however, correspond to $M_V = +6.7$. We conclude that they are all chance alignments, and will not discuss them further.

4.4. Caveats

As discussed in Paper II, the goal of the survey was to detect companions down to dwarf K spectral types, which limits contamination by field stars.

Table 2. Candidate Companions Detected after PSF Correction

Cepheid	Sep.	P.A.	m_{621} (raw)	m_{621} (corr)	σ_{621}	m_{845} (raw)	m_{845} (corr)	σ_{845}
	[arcsec]	[$^{\circ}$]	[mag]	[mag]	[mag]	[mag]	[mag]	[mag]
R Cru	1.9	344.5	15.43	15.36	0.03	14.41	14.33	0.02
U Aql	1.6	225.1	12.01	11.91	0.06	11.12	11.04	0.04
U Vul	1.5	319.7	16.26	16.18	0.04	14.92	14.85	0.03
S Nor	0.9	259.2	11.69	11.40	0.49	11.47	11.20	0.43
V659 Cen	0.6	234.9	10.54	–	–	10.12	–	–
η Aql	0.7	95.7	9.34	–	–	8.90	–	–
AX Cir	0.3	332.4	7.24	–	–	6.98	–	–
AV Cir	2.1	288.5	20.11	20.00	0.03	19.19	19.10	0.07
BG Cru	3.1	294.8	15.52	15.11	0.08	14.90	14.70	0.04
CO Aur	2.8	8.8	18.65	–	–	17.66	–	–

Table 3. Properties of Candidate Companions Detected after PSF Correction

Cepheid	Sep.	V	$V - I$	$(V - I)_0$	$E(B - V)$	Dist.
	[AU]	[mag]	[mag]	[mag]	[mag]	[pc]
R Cru	1580	16.02	1.49	1.27	0.19	829
U Aql	981	12.53	1.30	0.90	0.35	613
U Vul	822	16.85	1.79	1.04	0.65	548
S Nor	819	11.55	0.30	0.08	0.19	910
V659 Cen	452	–	–	–	0.21	753
η Aql	191	–	–	–	0.12	273
AX Cir	158	–	–	–	0.25	527
AV Cir	1472	20.63	1.34	0.88	0.40	701
BG Cru	1615	15.42	0.64	0.58	0.05	521
CO Aur	2229	19.30 uc	(1.45)	(1.19)	0.23	796

As discussed below (Table 5), in a number cases an absolute magnitude from other sources, such as *IUE* spectra, is more accurate than the *HST* photometry for very close companions.

5. CHANDRA OBSERVATIONS

Analysis of the properties of members of the multiple systems containing a Cepheid frequently requires multiwavelength observations. X-ray observations are often an important diagnostic. Specifically, *Chandra* observations of two stars R Cru and S Mus followup *XMM* observations in Paper IV with higher spatial resolution, providing additional information about system components. The details of the observations are provided in Appendix C.

6. DISCUSSION

6.1. Summary of Candidate Companions

Because of differences in the data-analysis procedures dictated by the angular separations, in the preceding work we divided the resolved companions found in our *HST* WFC3 imaging survey into three groups (separations $>5''$,

2–5", and <2"). In the following discussion, we will combine the first two groups, designating them the “*Resolved Wide*” companions. The latter group will be called the “*Resolved Close*” companions. In terms of physical projected separations, the Resolved Wide companions lie more than ~ 2000 AU from the Cepheid, and the Resolved Close ones are closer to the primary star. We now examine whether the properties of the stars in the two groups differ.

Table 4 presents the results for the combined sample of 16 candidate companions. These data are assembled from Table 2 in Paper II for the top group, with separations greater than 5". For the middle group, with separations of 2" to 5", the entries are from Table 1. The data for the close companions below 2" are more complicated, and these companions are discussed individually below. Our measures of separation and magnitude are listed in Tables 2 and 3. However, for very close companions, and systems with multiple companions, the most reliable companion parameters come from several sources, which are discussed and assembled in Table 5. Table 4 lists the projected separations in both arcseconds and AU, the V and $V - I$ magnitudes and colors, the dereddened $(V - I)_0$ color, the $E(B - V)$ reddening, and the distance. The distances and reddenings are from Paper II. As in Paper II, the $V - I$ color excess is found from the relation $E(V - I) = 1.15 E(B - V)$.

Among the possible companions separated by more than 5" from the primaries, only five systems remained after we eliminated those candidates undetected in X rays, implying that they are not young enough to be Cepheid companions. The remaining five are R Cru, FF Aql, AP Sgr, RV Sco, and TT Aql. The discussion in Paper II concluded that a Cepheid with a crowded line of sight (a field with more than two possible companions) is more likely to have chance alignments. On that basis we remove TT Aql. The candidate companion of AP Sgr has the second-largest physical separation in the remaining sample, and it is a K dwarf, which is the most common type of field-star chance alignment. Thus AP Sgr is the most suspect of the remaining retained candidates in the list. As discussed in Appendix C, we are retaining the candidate wide companion for R Cru.

We also checked the *Gaia* DR2 catalog for parallaxes and proper motions of our candidate companions. Because the candidates are so close to the much-brighter Cepheids, in most cases parallaxes are not available, particularly for the closer companions. The candidate companions of V737 Cen, R Mus, and Y Sgr were found to be much more distant than the Cepheids, consistent with the negative results of the X-ray observations reported in Paper IV; they are not included in Table 4. For the possible companions with separations $> 5''$ in Table 4, the DR2 results are as follows. The *Gaia* DR2 parallax for R Cru itself is negative, but the parallax of the wider of its two candidate companions is consistent with the distance given in Table 4 (and with the *Hipparcos* parallax of R Cru), and its DR2 proper motion is similar to that of the Cepheid. The parallax of the FF Aql companion agrees within the errors with that of the Cepheid, but as noted by Kervella et al. (2019b), its proper motion is significantly different; this implies a relative velocity too large for it to be bound, unless it is itself a binary. The companion for AP Sgr is listed in DR2, but no parallax is given. Finally, the DR2 parallax for the wider of the two RV Sco companions agrees with that of the Cepheid within the errors, and its proper motion is similar.

The middle group in Table 4 lists the candidate companions with separations between 2" and 5". The only companion listed in *Gaia* DR2 is that of RV Sco, but no parallax or proper motion is given. In the case of V496 Aql, the DR2 parallax is significantly smaller (4.3σ) than that of the Cepheid, and hence is likely to be a chance alignment. It has been omitted from Table 4.

6.2. Resolved Close Companions: Companions Closer than 2"

A number of the systems with a companion closer than 2" to the Cepheid have at least one additional component. This means disentangling the mass and temperature of the companions often requires information from a number of techniques. Here we discuss what is known about the components of these close systems in the third group in Table 4. This becomes important below, in first examining the CMD of the companions, and subsequently the distribution of colors as a function of separation, and the multiplicity properties of the sample.

Because massive star systems often have multiple components, in Appendix D we go into considerable detail about each system. Derivation of the parameters of each component (mass, temperature, and luminosity) can be done using observations over a wide wavelength range, and also as a function of separation. There are many approaches and tools currently available to do this. Radial-velocity studies extend over many decades. The emphasis in this study is on separations on the 1" scale, but a number of systems have been observed via interferometry (e.g., Gallenne et al. 2019), accessing closer separations. Both *HST* and *IUE* provide information about hot companions in the satellite ultraviolet. *Chandra* and *XMM* X-ray observations test the ages of companion candidates. Finally *Gaia* and *Hipparcos* data have contributed in two ways (Kervella et al. 2019a, 2019b). First, the comparison of proper motion from the two satellites

Table 4. Summary of Resolved Candidate Companions

Cepheid	Sep.	Sep.	V	$V - I$	$(V - I)_0$	$E(B - V)$	Dist.
	[arcsec]	[AU]	[mag]	[mag]	[mag]	[mag]	[pc]
Resolved Wide							
		Separation $> 5''$					
R Cru	7.6	6330	16.28	1.17	0.95	0.19	829
FF Aql	6.9	2520	11.22	0.85	0.60	0.22	365
AP Sgr	6.3	5320	17.85	1.72	1.50	0.19	845
RV Sco	6.0	4520	12.68	0.63	0.24	0.34	753
		$2'' < \text{Separation} < 5''$					
RV Sco	3.6	2710	16.00	1.34	0.95	0.34	753
BB Sgr	3.3	2740	18.08	1.77	1.45	0.28	831
Y Car	3.2	4700	17.40	1.29	1.20	0.08	1468
"	2.6	3820	16.91	0.93	0.84	0.08	1468
V350 Sgr	3.1	2780	17.91	1.77	1.40	0.32	896
Resolved Close							
		Separation $< 2''$					
R Cru	1.9	1580	16.02	1.49	1.27	0.19	829
U Aql	1.6	981	12.53	1.30	0.90	0.35	613
U Vul	1.5	822	16.85	1.79	1.04	0.65	548
S Nor	0.9	819	11.55	0.30	0.08	0.19	910
η Aql	0.7	191	—	—	—	0.12	273
V659 Cen	0.6	452	—	—	—	0.21	753
AX Cir	0.3	158	—	—	—	0.25	527

in some cases results in “proper-motion anomalies,” indicative of orbital motion. Second, comoving companions can be identified and classified either as bound or not. These data are discussed further in Section 6.9, “*Gaia* Components”.

In the discussion of some of the systems we have estimated masses of the companions. The approach used is discussed in Evans et al. (2018), based on data from detached eclipsing binary systems (Torres et al. 2010). In particular, since the companion to a more massive primary should not have evolved significantly, the lower envelope to the temperature–mass data is used.

Magnitude measurements for sources within $2''$ of the Cepheid have substantial uncertainties. This is particularly important in determining the color or temperature using the difference of two filters, resulting in an uncertainty which is a significant fraction of the range of color. In many cases for the companions, there is an alternate measurement which provides a more accurate color or temperature. Specifically, many of the stars have an *IUE* spectrum, which provides a sensitive determination of the spectral type of the companion; the companion can completely dominate the flux at 1500 \AA . Table 5 summarizes the best (“preferred”) combination of V_0 and $(V - I)_0$ available for the companions within $2''$ of the Cepheid. V_0 is taken from Table 3 for S Nor, R Cru, U Aql, and U Vul. From this, and the distance in Paper II, M_V is computed (column 3). Column 4 is the spectral type from the instruments and literature references in columns 6 and 7. Additional details are given for each star in Appendix D. The closest companions, V659 Cen B and AX Cir B, provide magnitudes which are too uncertain on the WFC3 images, so the value of M_V based on the *IUE* spectral type has been substituted. For η Aql, the M_V from the VLT/NACO imaging is in Appendix D.

This information for complex systems is discussed in Appendix D. We summarize the component parameters in Table 6 for reference. This includes the resolved companions (Table 5), as well as inner spectroscopic binaries and possible wider system members. While there is a lot of detail in the linked inferences, the available observations provide well constrained properties for most of the stars involved. The top entry for each Cepheid is for the resolved companion identified in this study. The second column is the binary/multiple star notation. V_0 , $(V - I)_0$, and M_V are taken from Table 5. The final right column lists results for very wide companion candidates from *Gaia* DR2 (Kervella

Table 5. Preferred Properties of Resolved Close Companions

Primary	V_0	M_V	Spec. Type	$(V - I)_0$	Source	Ref. ^a
(Cepheid)	[mag]	[mag]		[mag]		
	Comp	Comp	Comp	Comp		
R Cru	15.4	+5.8		1.27		(1)
U Aql	11.3	+2.4	A5	0.16 ^b	<i>HST</i> /STIS	(2)
U Vul	14.6	+5.9		1.04		(1)
S Nor	10.89	+1.1	B9.5 V	-0.04 ^b	<i>IUE</i>	(3)
V659 Cen	8.72	(-0.3)	B6.0 V	-0.16 ^b	<i>IUE</i>	(3)
η Aql	10.0	+3.2	F3	0.44 ^b	VLT/NACO	(4)
AX Cir	6.91	(-0.3)	B6.0 V	-0.16 ^b	<i>IUE</i>	(5)

^aReferences: (1) Table 4; (2) Appendix D (3) Evans 1992b; (4) Gallenne, et al.2014b (5) Evans 1994

^bFrom Drilling & Landolt 2000, their Table 15.11 (which is quoted from Bessell 1979).

et al. 2019b), where WB is bound companions, WC is comoving companions. Systems in Tables 5 and 6 are ordered by decreasing separation of the resolved companion.

The important characteristic that emerges from the discussion of the complex systems is that all the systems with Resolved Close companions (companions within $2''$) have an *interior spectroscopic binary* (or at least one is strongly suspected, in the case of S Nor). This is discussed in more detail in Section 6.6.

6.3. Resolved Close Companion Properties: CMD

We now return to a discussion of the close but resolved companions (Table 5), which are the first entry for each of the systems in Table 6 as discussed in Appendix D. As a first step in assessing the properties of the resolved close companions (within $2''$ of the Cepheid [Table 5]) we consider the CMD (Figure 6), which provides a first examination of the properties of these companions. The companions are fairly evenly distributed in color, M_V , and hence in mass. Unlike the field Initial Mass Function (IMF), they are not concentrated to low-mass stars. For wider companions, comparisons with the ZAMS are the way physical companion candidates are identified. In Figure 6 this is only a test for the two coolest companions, R Cru and U Vul, since they are the only ones which are based on WFC3 photometry. While these points sit above the ZAMS indicating some errors, they are consistent with the companions being low-mass stars.

6.4. Systems with a Resolved Wide Companion (Wider than $2''$)

Because the systems with a companion closer than $2''$ have the distinctive property of an inner spectroscopic binary (Table 6), we examine the multiplicity properties of the systems with a companion wider than $2''$ to see if they share this characteristic. Components of these systems are summarized in Table 7. Unless discussed below, the spectral types for the companions are derived from $(V - I)_0$ in Table 7, using the calibration of Drilling & Landolt (2000; their Table 15.11). The details of the components of these systems are discussed in Appendix F.

The possible companions with separations larger than $2''$ are more likely to contain a line-of-sight coincidence with an unrelated field star than the inner group. However, of the six Cepheids for which a possible companion has been identified in this group, five have strong evidence of an inner spectroscopic binary, and only for one (BB Sgr) is an inner binary questionable and it is a cluster member. That is, the resolved wide systems share this characteristic of the resolved close companions. This is an additional property consistent with physical system membership.

6.5. Distribution of Colors

Table 6. Multiple Components in Systems with Resolved Close Companions

Cepheid	Multiple	Sep.	Sep.	SB ^a	V_0	M_V	Spec.	Ref. ^b	Wide ^c
	ID	[arcsec]	[AU]		[mag]	[mag]	Type		
R Cru	AB	1.9	1580		15.4	+5.8	K	1	WB
	Aa,Ab		3:	SB			<A2	9	
	AC	7.6	6300		15.6	+6.0	K2 V	11	
U Aql	AB	1.6	981		11.3	+2.4	A5 V	6	
	Aa,Ab	0.107	66			+1.8	A3-4 V	6	
	Aa1,Aa2	0.0101	6.2	SB		+1.2	B9.8 V	6	
U Vul	AB	1.5	822		14.6	+5.8	K0	1, 9	
	Aa,Ab		7.1	SB			<A1	3, 9	
S Nor	AB	0.9	819		10.9	+1.1	B9.5 V	1, 10	WC
	Aa,Ab		8.87	SB:			F0 V	3	
	AC	14.6	13300		13.29	+3.5	G3 V	11	
V659 Cen	AB	0.6	452		8.7	-0.3	B6.0	1, 9	WB
	Aa,Ab		3:	SB				5	
η Aql	AB	0.7	191		10.0	+3.2	\sim F3 V	1, 2	
	Aa,Ab		1.3:	SB	8.39	+1.2	B9.8 V	4, 8	
AX Cir	AB	0.3	158		6.9	-0.3	B6.0	1, 9	WB, WC
	Aa,Ab	0.029	15.4	SB		+0.2	B9.0	7, 12	
	Ab1,Ab2							7, 12	

^a Spectroscopic Binary Companion^b References: 1: Table 5; 2: Gallenne et al. 2014a; 3: Kervella et al. 2019a; 4: Appendix C; 5: Anderson, R. I. 2020, in preparation; 6: Appendix D; 7: Gallenne et al. 2014b; 8: Evans 1991; 9: Evans 1992a; 10: Evans 1992b; 11: Paper IV; 12: Gallenne et al. 2020 in preparation^c Wide companion types: WB gravitationally bound; WC comoving.

Ultimately we want to examine the properties of possible companions as a function of the (projected) separation in AU, which is shown in Figure 7. Companion candidate properties are taken from Table 5 when available or from Table 4.

Companion candidates closer than 2000 AU span the full range of $(V - I)_0$. The hottest companion candidates, however, do not occur at larger separations. The hottest of the more distant companions, FF Aql and RV Sco [with $(V - I)_0$ colors corresponding approximately to G0 and A7 dwarfs, respectively] have evidence that they are associated with the Cepheid (Appendix F). The other companion candidates with separations larger than 2000 AU are all cooler (approximately K0 or later). Thus there appears to be a trend in the color or temperature and mass of the companion candidates to less-massive stars at wider separations. This raises the question whether wider companions actually are preferentially less massive (or have been dynamically “widened”), or whether they are chance alignments with field stars or possibly a mixture of both.

One of the goals of this study is to determine how far from the Cepheid physical companions occur. The diminishing number with separations greater than 6000 AU is consistent with the results of X-ray studies to identify active stars young enough to be Cepheid companions. X-ray observations of 14 of the 39 Cepheids with companion candidates with separations greater than $2''$ in Paper II were discussed in Paper IV. The only two Cepheids with X-ray confirmed companions greater than 6000 AU were R Cru (above) and S Nor. However, since S Nor is in a cluster the X-ray source may be a cluster member rather than a gravitationally bound companion. Possible wide but bound companions revealed by *Gaia* are discussed in Section 6.9. Seven Cepheids in the WFC3 survey (δ Cep, AX Cir, AW Per, V350

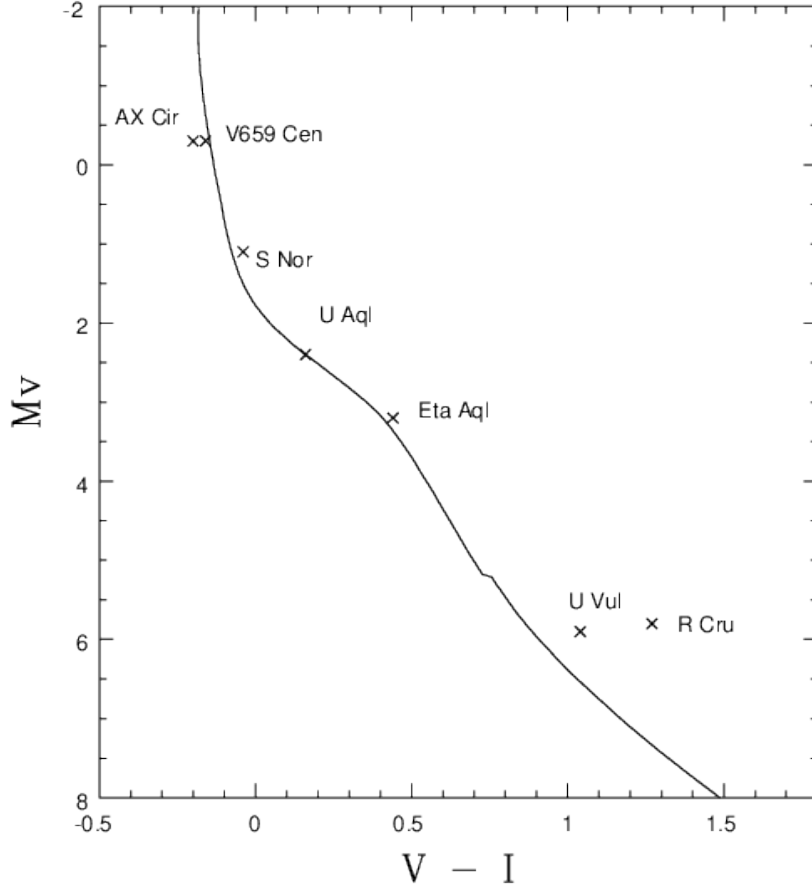


Figure 6. The M_V versus $(V-I)_0$ color-magnitude diagram for the resolved close companions (Table 5). Colors and magnitudes are from Table 5, for which most are taken from WFC3 images. For η Aql, the data are from Gallenne et al. (2014a), although it agrees with the WFC3 data. For AX Cir and V659 Cen, data are from *IUE* spectra. Identifications of the stars are included on the plot. The solid line is the ZAMS from Paper II.

Sgr, V659 Cen, BP Cir and V950 Sco) have possible companions (Tables 9 and 10) as does the cluster Cepheid U Sgr. This hints at further extended low-density companions.

6.6. Multiplicity

The group of stars with resolved close companions contains companions which are highly likely to be physically related to the Cepheid. As discussed above, the systems are complex, and it requires a number of approaches in addition to the *HST* WFC3 observations to build up a picture of the masses and separations of the components. Table 6 summarizes the information on the members of each system. In addition, as discussed in Section 6.9, Kervella et al. (2019b) used *Gaia* data to identify wide companions from distances and proper motions and test whether they are likely to be gravitationally bound to the Cepheid. The final right-hand column in Table 6 indicates whether a wide bound (WB) or wide comoving (WC) companion candidate was found.

Figure 8 further summarizes the components schematically. We stress that it was developed from the list of Cepheids with resolved companions at separations of typically a few hundred AU (Table 6). It is striking that in the Cepheid list compiled in this way, **all** have evidence of an inner binary, often with a known orbit. As noted above, because S Nor is in a cluster it may have a different history of formation or interaction than the field stars and also possible chance alignments with cluster stars. Precise masses are not available for all the companions; however limits or estimates can often be made from spectral types (Table 6). Figure 8 shows the masses schematically either as comparable to the Cepheid itself (a B star: large blue squares) or a lower-mass A, F or G star (small red squares). While this is a

Table 7. Multiple Components in Systems with Resolved Wide Companions

Cepheid	Multiple	Sep.	Sep.	SB ^a	V_0	$(V - I)_0$	M_V	Spec.	Ref. ^b	Wide ^c
	ID	[arcsec]	[AU]		[mag]	[mag]	[mag]	Type		
AP Sgr	Aa,Ab		12:	SB:				$\leq A5$	5,2,4	
	AB	6.3	5320		17.19	1.50	+7.56	K7	3	
Y Car	Aa,Ab	0.0025	3.6	SB				B9.0 V	6,7,4	WC
	AB	2.6	3820		16.63	0.84	+5.80	K0	3	
or	AB	3.2	4700		17.12	1.20	+6.29	K5	3	
RV Sco	Aa,Ab		14:	SB				$< A3$	4,2	
	AB	6.0	4520		11.50	0.24	+2.12	A7 V	3	
or	AB	3.6	2710		14.82	0.95	+5.44	K2 V	3	
V350 Sgr	Aa,Ab	0.0030	2.7	SB				B9.0 V	8,9	WB, WB
	AB	3.1	2780		16.80	1.40	+7.04	K6	3	
BB Sgr	AB	3.3	2740		17.11	1.50	+7.51	K7	3,4,5	
FF Aql	Aa,Ab	0.0082	4.5	SB				K0	1,4	
	AB	6.9	2520		10.46	0.60	+2.65	G0 V	3	

^aSpectroscopic Binary Companion^bReferences: 1. Gallenne et al. 2019; 2. Evans 1992a; 3. Table 4; 4. Kervella et al. 2019a; 5. Szabados 1989; 6. Petterson et al. 2004; 7. Evans et al. 2005; 8. Evans et al. 2018; 9. Kervella et al. 2019b.^cWide companion types: WB gravitationally bound; WC comoving.

crude division, several things are apparent in Figure 8. There is a variety in the component masses. For instance, R Cru and U Vul have only lower-mass companions, whereas other systems have a mixture of masses. For AX Cir and V659 Cen, the most massive companion is not the closest companion (Section 6.2). The more massive companions are typically the closer ones, although AX Cir and V659 Cen are exceptions. This might be due to the formation process or subsequent dynamical evolution.

It is surprising that all the systems with resolved close companions in Table 6 also have an inner binary system, or at least a suspected one. This is markedly different from the fraction of spectroscopic binaries among Cepheids with periods less than 20 years, which is $29\% \pm 8\%$ (Evans et al. 2015), less than a third of a Cepheid sample. In a scenario where systems with wider separations are formed before more closely separated components (in a process such as core fragmentation and subsequent disk fragmentation) it is hard to explain how wide components “know” an inner binary will be formed later. A more probable explanation for the *requirement* that a wide component in Figure 8 has an inner binary is that the wide component of the triple (or higher) system was moved outwards through dynamical interactions.

The resolved close companions in Figure 8 all appear to be distant third stars in triple systems. Because they are the closest resolved companions in the survey, they are the most likely to be gravitationally bound to the Cepheids. However, the striking result in Figure 8 of inner spectroscopic binaries encouraged us to check the slightly more distant resolved wide companions (from $2''$ to $7''$). System parameters are summarized in Table 7, and represented schematically in Figure 9. The system summaries in Figure 9 have been simplified in two ways. For two stars from Table 7 (RV Sco and Y Car), there are two possible companions in this range. Since it is dynamically unlikely that they are both system members because they are at very similar apparent separations, Figure 9 shows only the one considered to be the most probable. Second, wider companions discussed below are not shown. From the discussion of the Cepheids with resolved wide companions above (Table 7) all except BB Sgr have good evidence of an inner spectroscopic binary system. In addition, as with S Nor, BB Sgr is a cluster member. This provides an alternate possibility for the resolved wide companion, a chance alignment with a cluster member, rather than a bound system member. It is also notable that the outer companion is significantly less massive than the Cepheid. This again fits the

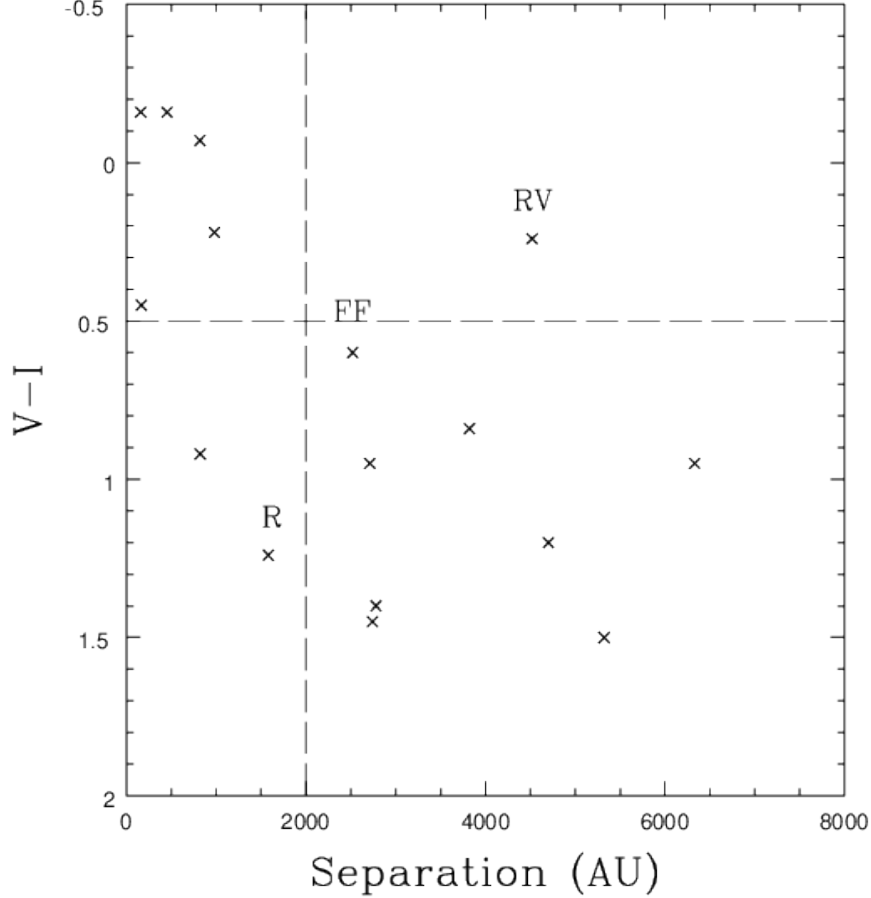


Figure 7. Colors and separations of the resolved close companions from the Cepheids. $(V - I)_0$ is in mag. The horizontal and vertical dashed lines are arbitrary divisions of the companion properties, for discussion purposes. A component of the R Cru, RV Sco, and FF Aql systems is indicated.

picture that a resolved companion with a projected separation of several thousand AU was moved outward through dynamical interactions within the triple system.

6.7. Dynamical Stability

The inner spectroscopic binaries for the 13 Cepheids in Tables 6 and 7 certainly have long-term dynamical stability with respect to the resolved companions from the WFC3 survey because of the very different orbital periods. However, two stars in Table 7 (RV Sco and Y Car) have two companions which have separations from the Cepheid which correspond to period ratios much less than 5, found by Tokovinin (2018b) in stable triple systems. Anticipating the *Gaia* results for likely wide but bound companions, V350 Sgr may also have two similar companions. While future studies may rule out one of these possible companions, and hence remove the question of stability, the fact that half the stars in Table 7 are in this situation may reflect something about star formation. One way to have a pair of companions at apparently similar separations but in a stable configuration is if they are not coplanar, but have very different inclinations. In summary, RV Sco, Y Car, and V350 Sgr may provide a clue to additional complexity in the formation processes.

The population of triple systems can have important effects on the evolution of the systems, such as in the Kozai-Lidov mechanism (Naoz 2016) as discussed in Section 6.10

6.8. Detection Probability

The following example provides an indication of the completeness of the survey. For a typical distance in the WFC3 survey (700 pc) and a typical reddening [$E(B - V) = 0.20$; Paper II], we estimate apparent magnitudes for a range of

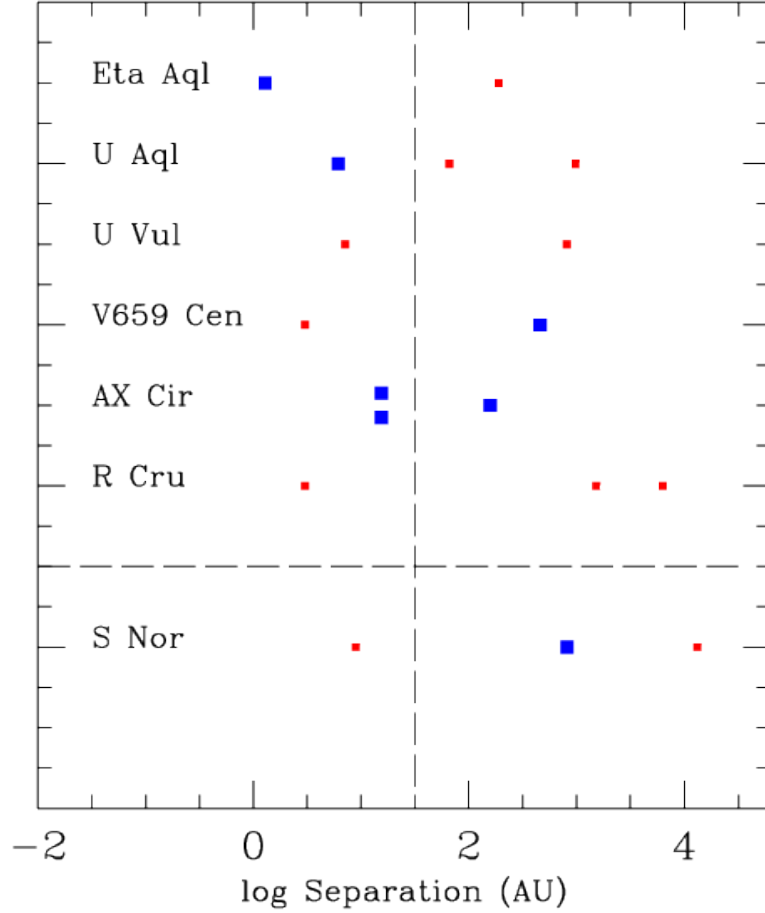


Figure 8. Schematic of the separations of companions from the Cepheids for resolved close companions (within $2''$) from Table 6. The vertical dashed line separates the spectroscopic companions (to the left of the line) from the resolved companions (to the right). Blue (large) and red (small) symbols represent companions earlier and later than A0 respectively. S Nor (below the horizontal dashed line) is a cluster member, and more difficult to interpret.

Table 8. Typical Magnitude for Probable Detection

Spectral	M_V	V at 700 pc ^a
Type	[mag]	[mag]
B9 V	+0.2	10.1
A3 V	+1.5	11.4
K0 V	+5.9	15.8

^a Assuming $E(B - V) = 0.2$

spectral types in Table 8; the M_V values are from Drilling & Landolt (2000). Using these magnitudes, the detection fraction from Figure 5 shows that nearly all the B9 and A3 companions would be detected outside $1''$. Later spectral types (K0) are severely missing inside $1''/6$. Thus, for the example of 700 pc, essentially all early-type companions would be detected at separations larger than 700 AU. For lower-mass companions, as represented by the K0 star, they would be largely detected only outside 1100 AU.

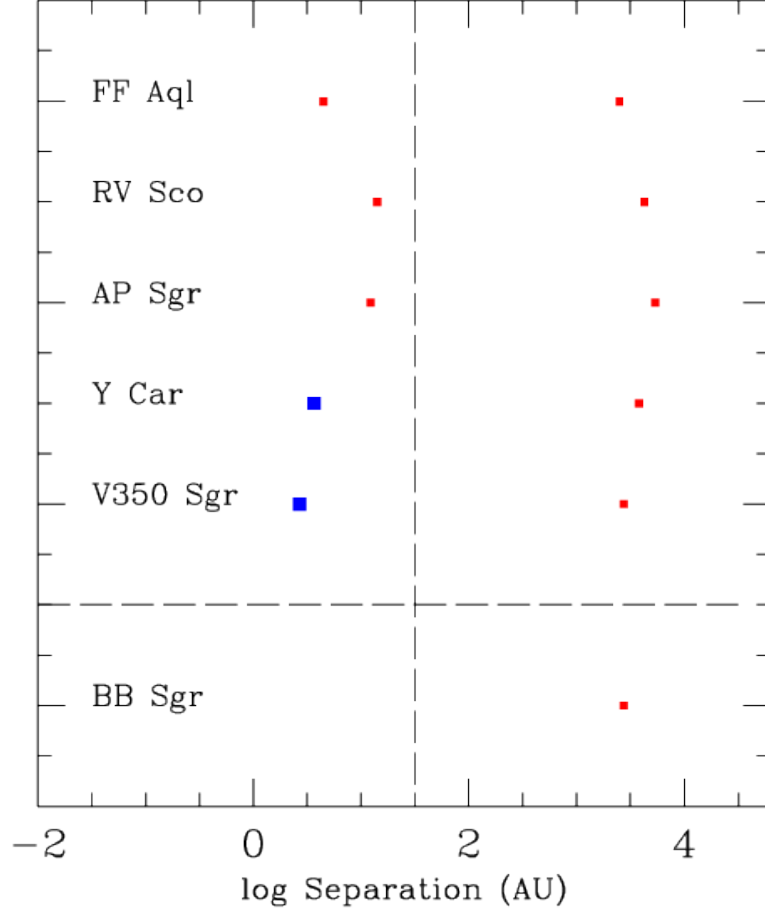


Figure 9. Schematic of the separations of companions for resolved wide companions (wider than $2''$). Symbols are the same as for Figure 8. BB Sgr (below the horizontal dashed line) is a cluster member.

6.9. Companions Identified by *Gaia*

The *Gaia* spacecraft has provided new data to investigate multiple systems, particularly to identify wide components from the outer regions of a star-forming cloud. This is also relevant to the question of whether there are stars formed at the same time which are neither gravitationally bound system members nor in a recognizable star cluster. In particular, studies have been done of proper motions to study orbits (Kervella et al. 2019a) and to identify wide companions (Kervella et al. 2019b)

Kervella et al. (2019a) have used the difference between proper motions from *Gaia* and *Hipparcos* to look for “proper-motion anomalies” resulting from orbital motion between the two epochs. Of the 70 stars in our WFC3 sample, they list data for 63, or 90%. (Of these 16, or 25%, had less-than-perfect *Gaia* data, often because the Cepheid is too bright.) The *Gaia* data showed proper-motion anomalies for 28 stars (44%) at the level of 2σ or greater, many of which are known spectroscopic binaries. We stress that this is only a first exploration of the *Gaia* results, which are expected to improve in the future. Specifically, other stars have indications of proper-motion anomalies, but at a lower significance level. As an example, S Mus is a well-known binary with an orbit, but does not meet the proper-motion-anomaly criterion.

6.9.1. Proper Motion Anomaly

Proper Motion Anomaly plus Orbit

Comparison of stars in the WFC3 survey and the *Gaia* proper-motion study is presented in Table 9, based on Tables A1, A2, and A3 in Kervella et al. (2019a), which lists the Cepheids which have proper-motion anomalies and orbits. The columns in Table 9 contain: 2 and 3: the semimajor axis in mas and AU; 4: whether there is a resolved companion

from Table 4 (Y); 5: whether a gravitationally bound (B) companion or a wide (W) comoving companion has been identified (see below); 6 and 7: the separation for a gravitationally bound companion in AU and mas; 8: the spectral type of the companion; 9 and 10: the separation for a comoving companion (W), and its spectral type; and 11: whether the star is a cluster member (C) from Anderson (2013). The semimajor axes are from Kervella et al. (2019a; Table 2). Because of the additional information from *Gaia*, particularly the individual parallaxes (which will be updated in DR3), they differ somewhat from the values in Table 6. Approximate spectral types have been inferred from the temperatures using the calibration of Pecaut & Mamajek (2013). (The symbol < M means cooler than M spectral types.) Two stars appear in Table 4 but not in either Tables 9 or 10 (η Aql and BB Sgr). For η Aql the *Gaia* quality flags are poor, probably because it is very bright, so the information on a proper-motion anomaly is also poor. BB Sgr has no proper-motion anomaly and no wide companions.

When a spectroscopic orbit is known, the proper motions allow the orbit to be fully determined, including the inclination. By assuming a mass for the Cepheid, a mass for the secondary can be determined. In Table 9 we list the semimajor axes in AU and mas for stars with orbits (from Kervella et al. 2019a Table 2). Even when spectroscopic orbits are available, those shorter than 1000 days are considered preliminary (marked with :).

Proper Motion Anomaly without Orbit

In addition to the stars in Table 9 a number of stars were found to have a proper-motion anomaly which do not have an orbit: AV Cir, T Cru, X Cyg, β Dor R Mus, AP Pup, RV Sco, SZ Tau, LR TrA, AH Vel, and T Vul. However, for a number of these stars, the *Gaia* parameters are imperfect (X Cyg, β Dor, AP Pup, and T Vul).

It is likely that many of these have longer-period orbits than stars for which orbits are known. This means they are likely to sample the orbital period range of the WFC3 stars with resolved close companions (Table 3), making this range accessible by a second technique. Further information on these stars, for instance from subsequent *Gaia* releases, is expected to provide new results for several sources, partly because the errors on the separations are large. For instance, X Cyg, SZ Tau, and T Vul (which have proper-motion anomalies) have accurate radial-velocity data which does not indicate orbital motion for periods less than 20 years (Evans et al. 2015). On the other hand, T Vul has a hot companion, which must be in a wider binary orbit (Evans et al. 2013). T Cru and AH Vel are found by Bersier (2002) to be binaries. However, Gallenne et al. (2019) had difficulty identifying an orbital period from new velocity data. LR TrA shows orbital motion (Szabados et al. 2013). There is also some evidence of orbital velocity variation for R Mus, AP Pup, and RV Sco, as discussed by Szabados (1989). All the stars in this section (except AV Cir and LR Tra) have been observed with *IUE* to search for hot companions. Only T Vul was found to have such a companion. The other stars had upper limits on spectral types in the early A range, corresponding to companions less massive than 2.9 to 2.0 M_{\odot} . The whole group warrants further velocity observation; however, orbital periods of more than 20 years are difficult to determine because they require a long time span of very accurate velocities.

There is a striking difference between system multiplicity of the proper motion anomaly stars with and without orbits. In Table 9, the stars with orbits frequently have resolved companions from the WFC3 survey. In the group without orbits, only RV Sco has a WFC3 resolved companion. Furthermore, stars with orbits frequently have a *Gaia* companion either bound or comoving. None of the stars without orbits have these companions. Only X Cyg is identified as a cluster member by Anderson (2013).

No Proper Motion Anomaly

In addition to the stars with a proper motion anomaly (Table 9 with orbits, and those without a known orbit), a number of stars in the WFC3 sample showed no proper-motion anomaly in the *Gaia* analysis. In the case of η Aql, RT Aur, l Car, V659 Cen, ζ Gem, T Mon, S Mus, W Sgr, Y Sgr, and X Vul the *Gaia* astrometry in DR2 has large uncertainties, often because the stars are bright. The following stars have good astrometry solutions, but no proper-motion anomalies: TT Aql, V636 Cas, V Cen, V737 Cen, IR Cep, S Cru, BG Cru, DT Cyg, W Gem, BF Oph, V440 Per, RS Pup, MY Pup, BB Sgr, V482 Sco, S TrA, V Vel, and SV Vul.

6.9.2. Wide Bound and Comoving Companions

In addition to the proper-motion anomalies, Kervella et al. (2019b) have used *Gaia* data to identify more widely separated companions. Candidates are selected because the companions and Cepheids have similar parallaxes, small differential tangential velocities, and small projected linear separation. (The list is drawn from Table 1 in Kervella et al. 2019b for companions rated likely on the basis of visual inspection.) They further divide the candidates into gravitationally bound companions and unbound but comoving companions based on differential tangential velocities.

These companions are added to the entries in Table 9 if the Cepheids also have proper-motion anomalies, or are listed in Table 10 if they have no proper-motion anomalies. The top three entries in Table 10 (V659 Cen, R Cru, and Y Sgr) have imperfect *Gaia* quality parameters, so their status might change in the DR3 release. In Table 10, V659 Cen and R Cru have spectroscopic-binary companions as previously discussed. BP Cir also shows orbital motion (Anderson et al. 2020, in preparation). As can be seen in Table 9, few of the Cepheids with proper-motion anomalies have *wide comoving* companions. This is also true of the whole sample in Kervella et al. (2019b), where there are also distinctly fewer comoving companions than bound companions. (These wide companions would not, in general, have been in the field of our WFC3 survey.)

The comoving wide companions provide a first opportunity to consider companions formed at the same location as the intermediate-mass Cepheids, but independent of the binary-star formation process. This is a part of star formation that we have been unable to explore previously because of the difficulty of recognizing a single star as compared with a gravitationally bound companion or a cluster. It is possible that some of the gravitationally bound candidates may ultimately be reassigned to the comoving group since the present analysis does not include radial-velocity information.

The occurrence of wide but gravitationally bound companions in Tables 9 and 10 varies markedly between the groups. In Table 9 (proper-motion anomaly with an orbit), 4 out of 17 systems (23%) have wide bound companions (B). The companions in this group have a range of spectral types from B through M, similar to the companion spectral types in Figure 6. Thus the companions do not appear to be dominated by field-star “impostors.” In Table 10 (no proper-motion anomaly but a wide companion or comoving star), 5 systems have a gravitationally bound companion. This makes a total of 9 systems with a wide companion, or 13% of the whole WFC3 sample. The fact that the fraction of wide gravitationally bound companions is smaller in the whole WFC3 sample than in the subsample with proper-motion anomalies and orbits (Table 9) could be due to a different density in the star-forming environment.

For the comoving candidate companions, there is no particular reason to relate their occurrence to the details of the multiple systems. The comoving candidates, however, are heavily dominated by K and M dwarfs. This is similar to the color distribution of companions at more than 2000 AU in Figure 7, indicating a larger fraction of “impostor” field stars, a change in properties of companions produced in star formation, or a dynamical evolution in multiple systems pushing smaller members outward.

We summarize the results for the Cepheids in the WFC3 study with resolved close and resolved wide companions in Table 11. The Tables from which the separations are taken is indicated. Three stars (Y Car, RV Sco, and V350 Sgr) have two possible companions with roughly the same separation from the Cepheids, making it dynamically unlikely that both are physical companions. We have marked one of the companions as an alternate (alt). As noted in Table 6 and Figure 8 stars with a close resolved companion also have an inner spectroscopic binary. It is also notable that three of the seven (or six, omitting S Nor) have wider gravitationally bound candidates, or 43 or 50%, much larger than the Cepheid sample as a whole (9 systems or 13%). Of the six resolved wide companions sample in Table 11 only one has a *Gaia* bound companion.

6.10. Multiplicity: Implications

Triple stars can form via two modes. First is an “outside-in” process, whereby core fragmentation on large scales initially produces the wide companions with $a_{\text{out}} > 100$ AU, followed by disk fragmentation on smaller scales that forms the close inner binaries with $a_{\text{in}} < 100$ AU (Moe & Di Stefano 2017; Tokovinin 2017). Second is an “inside-out” process, where two companions fragment within the same disk near $a_{\text{in}} \simeq a_{\text{out}} \simeq 10$ AU in an initially unstable configuration, and then subsequent dynamical interactions throw one of the components (typically the least-massive) to larger separations or eject it entirely (Reipurth & Mikkola 2012; Moe & Kratter 2018). The Kozai-Lidov mechanism (Naoz 2016) also results in dynamical evolution of the system.

As discussed in Section 6.6, all companions to Cepheids with separations from 100 to 2,000 AU, and nearly all companions with separations between 2,000 and 7,000 AU, are outer tertiaries to inner spectroscopic-binary companions with separations from 1 to 20 AU. The strong link between outer tertiaries and inner binary companions to Cepheids suggests a causal link, e.g., the dynamical-unfolding scenario. Nearly all of the outer tertiary companions are less massive than the inner spectroscopic binary companions, consistent with the triple-star dynamical-unfolding scenario. In this dynamical-unfolding scenario, the outer tertiaries are expected to be highly eccentric, which may be tested in the future with *Gaia* astrometry.

Nonetheless, correlation does not necessarily imply causation. The binary fraction of O-type (Sana et al. 2014) and early-B (Moe & Di Stefano 2017) stars is nearly 100% within $a < 100$ AU, and therefore nearly all wide companions

Table 9. System Information from *Gaia*: PM Anomaly

	Sep	Sep	Res	Wide	B Sep	B Sep	SpTy	W Sep	SpTy	Clust **
	mas	AU	Comp	Comp	AU	mas		AU		
PM Anomaly: Orbits										
U Aql	5.64	20.47	Y							
FF Aql	4.47	8.22	Y							
V496 Aql	3.83	3.72								
RX Cam	4.21	3.41								
Y Car	3.73:	2.57:	Y	W				32300	K6 V	
SU Cas	1.65:	3.54:								
δ Cep	5.85	19.86		B	10800	40740	B7-8 III-IV +F0 V			
AX Cir	14.66	26.00	Y	B, W	42500	81490	M3.5 V	23000	M3 V	
SU Cyg	2.73:	3.27:		W				34400	K6 V	C
V1334 Cyg	6.18	7.29		W				43700	< M	
S Nor	8.87	9.67	Y	W				41100	K3 V	C
				W				38800	–	
S Sge	3.08:	2.07:								
X Sgr	2.40:	8.32:								
AW Per	27.22	29.15		B	8400	10270	K3.5 V			
V350 Sgr	5.16	5.24	Y	B	26200	29850	A2 V			
				B	30600	34920	K4.5 V			
V636 Sco	4.59	4.61								
U Vul	7.15	7.74	Y							

B Sep: Separation for gravitationally bound companions

W Sep: Separation for Comoving Companions

** From Anderson

beyond $a > 100$ AU to massive stars are outer tertiaries in hierarchical triples. Similarly, Evans et al. (2005) showed that triples are quite common among Cepheids, and again Evans et al. (2015) found that 30% of Cepheids have companions for a between 1 and 20 AU, probably because Cepheids began life as *late* B stars. In addition B stars in short-period orbits will have merged before the Cepheid stage, removing them from the binary statistics. The preponderance of Cepheids in hierarchical triples with a_{in} between 1 and 20 AU and a_{out} between 100 and 7000 AU could simply be due to the efficient formation of companions to massive stars via both disk fragmentation and core fragmentation on small and large scales, respectively. On the other hand, the estimates in Tables 6 and 7 show that the spectroscopic companions are within 20 AU, the regime well studied in Evans et al. (2015). The binary fraction from that study is 30%. Thus, in Table 6, of the 7 Cepheids with companions 2 would be expected to have spectroscopic-binary companions, rather than all 7. Similarly, in Table 7, 2 of the 7 stars would be expected to have companions in this range rather than 6. In sum, 13 of these 14 stars have spectroscopic companions within 20 AU, where 4 are expected, strongly implying that the system structure (triples) is not produced by the standard “outside-in” process.

Wide companions that derive from core fragmentation have systematically lower masses than inner binary companions that come from disk fragmentation (Moe & Di Stefano 2017). That is the case for Tables 6 and 7. Our wide tertiaries are systematically less massive than the inner binaries, but are still top-heavy compared to random pairings from the IMF.

Although a significant majority of *very* wide companions to solar-type stars are tertiaries, Tokovinin (2017) argued that most derive from fragmentation of adjacent cores, not dynamical unfolding, and therefore there is no causal link between inner binaries and outer tertiaries. This is related to the possibility that some Cepheids are the remnants of dispersed clusters (Anderson & Riess 2018). The identification of wide binaries formed from separate but adjacent

Table 10. System Information from *Gaia*: Bound and Comoving Companion Candidates

	Res	Wide	B Sep	B Sep	SpTy	W Sep	SpTy	Clust**
	Comp	Comp	AU	mas		AU		
No PM Anomaly								
V659 Cen*	Y	B	48300	62220	M3 V			
R Cru*	Y	B	6600	7700	G8 V			
Y Sgr*		W				33300	< M	C
		W				44300	--	
BP Cir		B	39000	66300	M2 V	48700	M9 V	
						33500	M3 V	
						29100	M2 V	
Y Oph		W				44000	K4 V	
U Sgr		B	43100	71990	A0 IV-V	40000	M0 V	C
		B	46100	76960	A0 V	21200	K7 V	
V950 Sco		B	15000	16070	G1 V	15800	G2 V	
						27300	K3 V	
R TrA		W				32600	K1 V	

B Sep: Separation for gravitationally bound companions

W Sep: Separation for Comoving Companions

* *Gaia* quality parameters imperfect

** From Anderson

cores derives from the fact that beyond about 10,000 AU, the number of companions increases strongly, beyond those presumably formed by core or disk fragmentation. Insight here comes from the *Gaia* wide companions. Wider companions from *Gaia* (Tables 9 and 10) from adjacent cores are expected to show some degree of correlation in component masses compared to independent cores (Tokovinin 2017). The frequency of these very wide companions rises steeply beyond about 10,000 AU. Tables 9 and 10 show that 16 Cepheids have either bound or unbound *Gaia* companions, very similar to the 13 Cepheids with resolved companions in the WFC3 study. The most likely explanation is that the *Gaia* survey only extended to 50,000 AU, where core/disk fragmentation stars are mixed with adjacent core stars. This may be an indication of the density of the formation environment (Deacon & Kraus 2020).

In reality, both an “outside-in” formation via the relatively independent processes of core fragmentation followed by disk fragmentation and an “inside-out” mode via dynamical unfolding likely contribute to our Cepheid triple sample. The Cepheid sample discussed here contributes to the sample of massive triples needed to fully compare the companion mass distributions to the two different models and determine which scenario is dominant. As indicated above, astrometric orbital solutions (or at least a sense of relative orbital motion) of the outer tertiaries will also help constrain their formation mechanism.

7. SUMMARY FROM THIS SERIES OF PAPERS

This paper completes the discussion of the series reporting results of our *HST*/WFC3 two-color search for resolved companions of 70 Galactic Cepheids. In the present paper we identified candidate stars lying at separations between 0".5 and 5".0, and present a list of the most probable companions. Our major results from the series are summarized here.

1. Detection of companions of bright Cepheids lying within 2" requires sophisticated image processing. In our sample, seven Cepheids have companions within this range.

2. Discussion of the identifications, separations, and spectral types of the companions has been aided by *Chandra* observations of R Cru and S Mus, and also *HST*/STIS spectra of U Aql and AX Cir. We provide a discussion of components for these systems (R Cru, η Aql, S Nor, U Aql, U Vul, V659 Cen, and AX Cir).

Table 11. Summary: Separations for Systems with Resolved Companions

	Sep SB AU	Sep Res AU	B Sep AU	SpTy	W Sep AU	SpTy	Other AU	Clust**
Close	Table 6	Table 6	Table 9 / 10		Table 9 / 10		Table 6	
R Cru	3:	1580	6600	G8 V				
U Aql	6.2	981					66	
U Vul	7.1	822						
S Nor	8.87	819			41100 38800	K3 V –	13300	C
V659 Cen	3:	452	48300	M3 V				
η Aql	3.9:	191						
AX Cir	15.4 15.4	158	42500	M3.5 V	23000	M3 V		
Wide	Table 7	Table 7	Table 9 / 10		Table 9 / 10		Table 7	
AP Sgr	12:	5320						
Y Car	3.6	3820 alt 4700			32300	K6 V		
RV Sco	14:	4520 alt 2710						
V350 Sgr	2.7	2780	26200 alt 30600	A2 V K4.5 V				
BB Sgr		2740						C
FF Aql	4.5	2520						

B Sep: Separation for gravitationally bound companions

W Sep: Separation for Comoving Companions

alt: alternate: not both dynamically stable

** from Anderson

3. The $(V - I)_0 - M_V$ CMD shows that the companions are fairly evenly distributed in mass (as opposed to being dominated by low-mass companions). However, this may be partly because low-mass companions are more difficult to discover within $1''$ of the Cepheid. In contrast, companion candidates with wider separations are less massive than $1.5 M_\odot$. Cepheids with companions within $2''$ with separations of a few hundred AU comprise 10% of those in the survey.

4. It is particularly striking that companion candidates in the $0''.5$ to $2''.0$ range, corresponding to separations less than 2000 AU, all have an inner binary system. This is in contrast with the typical fraction of Cepheids in spectroscopic binaries of $29 \pm 8\%$ found in a velocity sample. It is also clear that the resolved companion may be either more or less massive than the spectroscopic-binary companions.

5. Companions wider than $2''$ also have an inner spectroscopic binary for all or most systems (Table 7 and Figure 9).

6. As discussed in Section 6.10, in a standard scenario, it seems more likely that the resolved companion is formed first in a core-collapse process, followed by the formation of the spectroscopic binary through disk fragmentation. In this scenario it is unlikely that the formation of the outer component can “anticipate” the formation of an inner binary. The most likely explanation that the resolved companion seems to “require” a spectroscopic binary is that that combination results from dynamical evolution, which can, of course, occur in triple systems. However, processes of “outside-in” formation, adjacent cores, and the dissolution of clusters may be involved in some cases.

7. In order to put the Cepheid multiple systems in context, we have also used *Gaia* results to incorporate proper-motion anomalies into orbits (Kervella et al. 2019a) and to identify wider companion candidates (gravitationally bound and comoving; Kervella et al. 2019b). The occurrence of wide companions is about 14%.

This paper focuses on Cepheids with companions at separations from approximately 100 AU to several thousand AU. This group has several characteristics relevant to the formation of multiple stellar systems. All have an inner (spectroscopic) binary. The distribution of companion spectral types (temperatures) or masses is distinctly different for companions within about 2000 AU and those at wider separations (Fig. 7). As discussed in Item 6 above, the properties of companions provide clues to the formation and evolution of the systems. Thus, although the properties of companions in multiple systems are difficult to obtain, this group warrants further observation.

ACKNOWLEDGMENTS

This research is based on observations made with the NASA/ESA *Hubble Space Telescope* obtained from the Space Telescope Science Institute, which is operated by the Association of Universities for Research in Astronomy, Inc., under NASA contract NAS 5-26555. These observations are associated with program 12215, with support for this work was provided by NASA through grants from the Space Telescope Science Institute (GO-12215.01-A and GO-13368.01-A). Support was provided to NRE by the *Chandra* X-ray Center NASA Contract NAS8-03060, and for NASA grants for proposal 17200363. Support for this work was provided by the National Aeronautics and Space Administration through the Smithsonian Astrophysical Observatory contract SV3-73016 to MIT for Support of the Chandra X-Ray Center, which is operated by the Smithsonian Astrophysical Observatory for and on behalf of the National Aeronautics and Space Administration under contract NAS8-03060. The authors acknowledge the support of the French Agence Nationale de la Recherche (ANR), under grant ANR-15-CE31-0012-01 (project UnlockCepheids). The research leading to these results has received funding from the European Research Council (ERC) under the European Union’s Horizon 2020 research and innovation program (grant agreement No. 695099). This work has made use of data from the European Space Agency (ESA) mission *Gaia* (<https://www.cosmos.esa.int/gaia>), processed by the *Gaia* Data Processing and Analysis Consortium (DPAC, <https://www.cosmos.esa.int/web/gaia/dpac/consortium>). Funding for the DPAC has been provided by national institutions, in particular the institutions participating in the *Gaia* Multilateral Agreement. The SIMBAD database, and NASA’s Astrophysics Data System Bibliographic Services were used in the preparation of this paper.

Facilities: *HST* (WFC3) *Chandra*

Software: DrizzlePac (Hack, et al. 2012), Astropy (The Astropy Collaboration 2013), DAOPHOT (Stetson, P. 1987), Sherpa (Freeman, et al. 2001; Doe, et al. 2007) Photutils (Bradley, L. et al. 2019), and IRAF (Tody, D. 1986, 1993)

APPENDIX

A. CANDIDATE COMPANIONS WITH SEPARATIONS BETWEEN $2''$ AND $5''$: RESOLVED WIDE COMPANIONS

The images and CMDs for companion candidates with separations between $2''$ and $5''$, discussed in Section 3, are presented in this Appendix. The CMDs include stars from the full WFC3 images, but the companion candidates indicated by arrows are only from the $2''$ to $5''$ region.

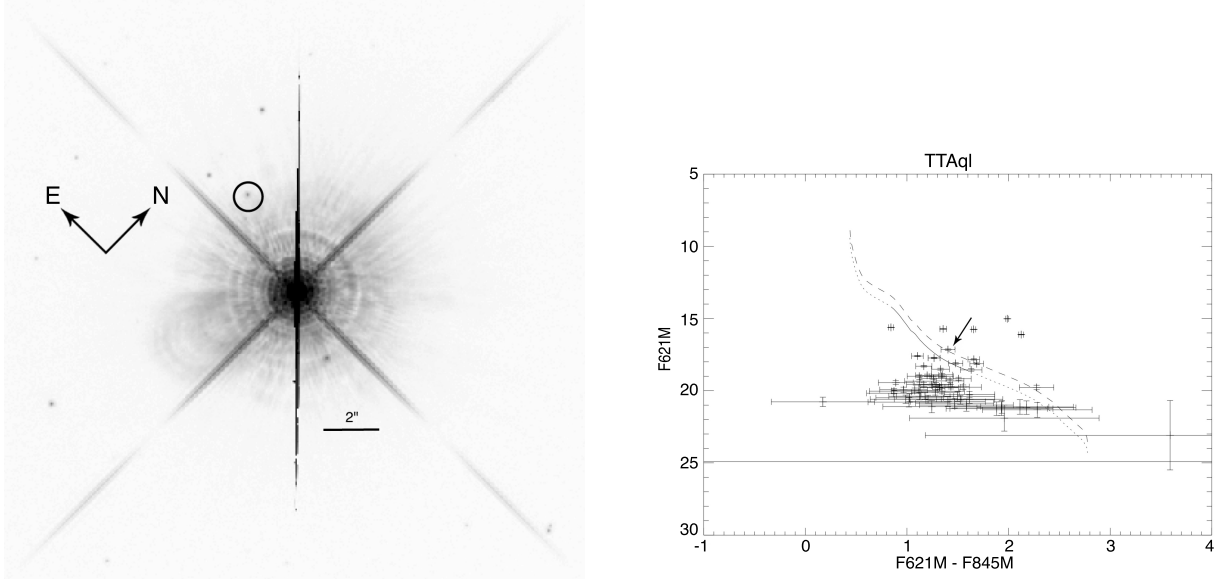


Figure 10. (left) The inner portion of the F845M WFC3 image of TT Aql. The possible companion is circled. A log scale is used, and $2''$ is indicated by the bar. (right) The CMD from the F845M and F621M WFC3 images. The lower line is the ZAMS at the distance and with the reddening of the Cepheid. The solid portion is the spectral region of F2 to K7; dotted parts are the extension to other spectral types. The dashed line is 0.75 mag brighter to include binaries. The arrow perpendicular to the ZAMS indicates the possible companion. Other stars within this band are more widely separated from the Cepheid which were discussed in Paper II.

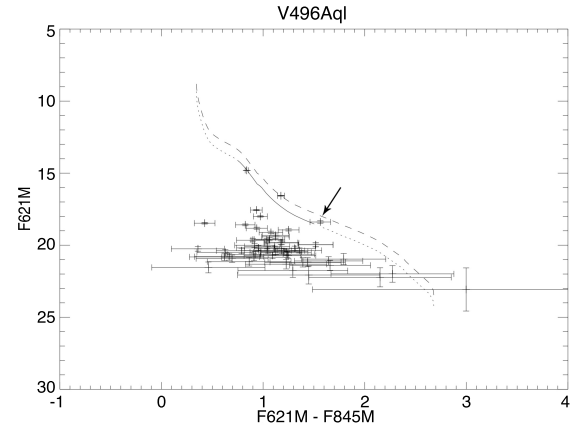
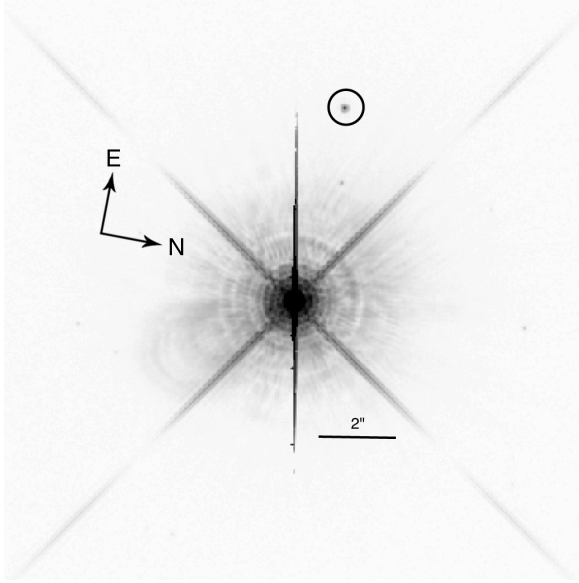


Figure 11. (left) The inner portion of the F845M WFC3 image of V496 Aql. The possible companion is circled. A log scale is used, and $2''$ is indicated by the bar. (right) The CMD from the F845M and F621M WFC3 images for V496 Aql. Symbols are the same as for Figure 10.

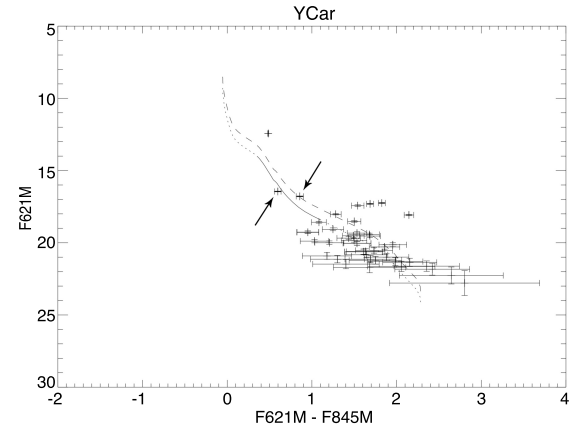
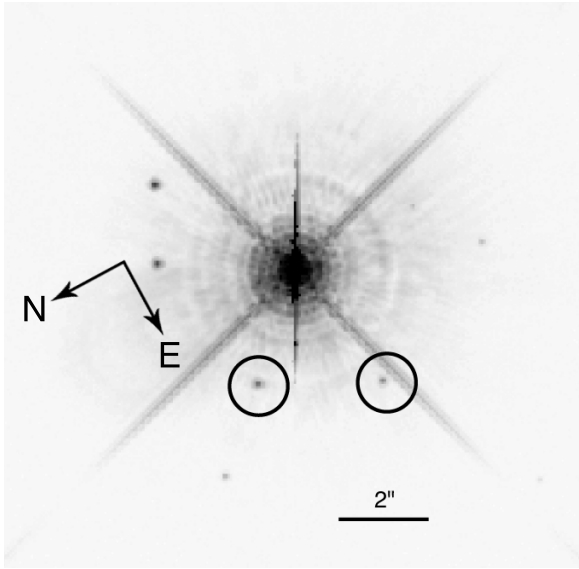


Figure 12. (left) The inner portion of the F845M WFC3 image of Y Car. The possible companions are circled. A log scale is used, and $2''$ is indicated by the bar. (right) The CMD from the F845M and F621M WFC3 images for Y Car. Symbols are the same as for Figure 10.

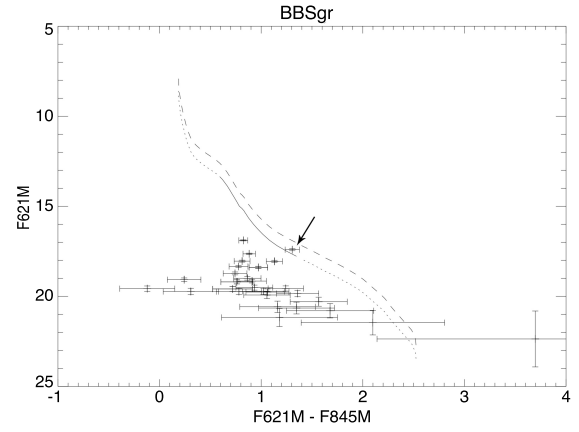
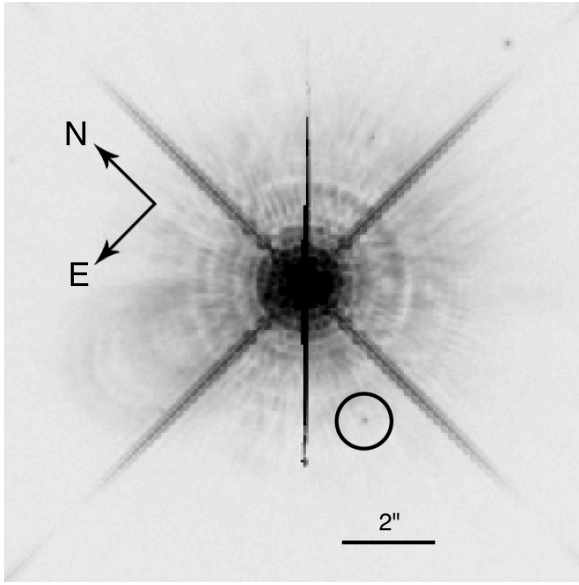


Figure 13. (left) The inner portion of the F845M WFC3 image of BB Sgr. The possible companion is circled. A log scale is used, and $2''$ is indicated by the bar. (right) The CMD from the F845M and F621M WFC3 images for BB Sgr. Symbols are the same as for Figure 10.

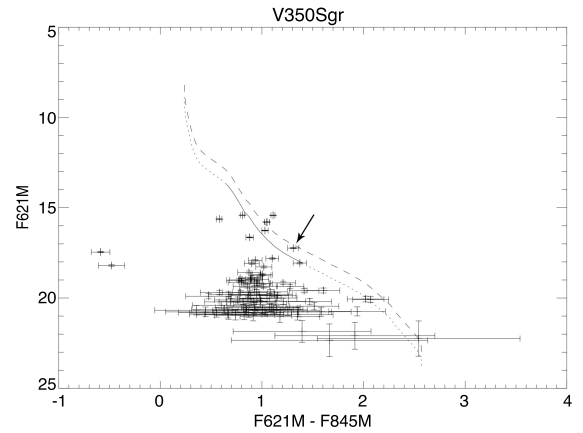
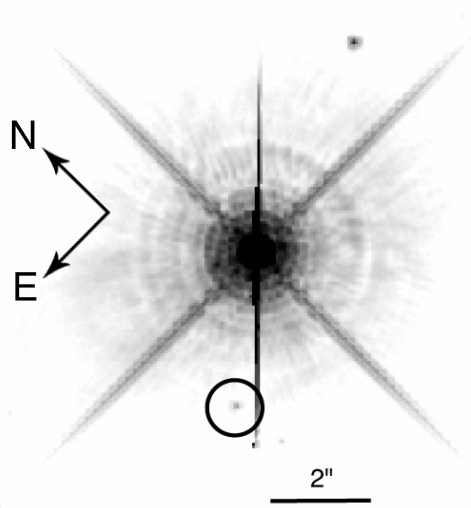


Figure 14. (left) The inner portion of the F845M WFC3 image of V350 Sgr. The possible companion is circled. A log scale is used, and $2''$ is indicated by the bar. (right) The CMD from the F845M and F621M WFC3 images for V350 Sgr. Symbols are the same as for Figure 10.

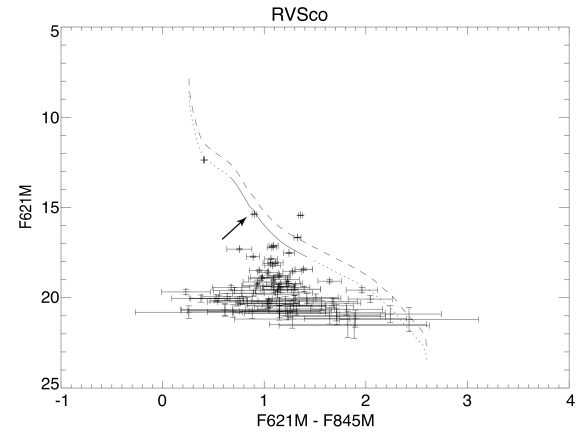
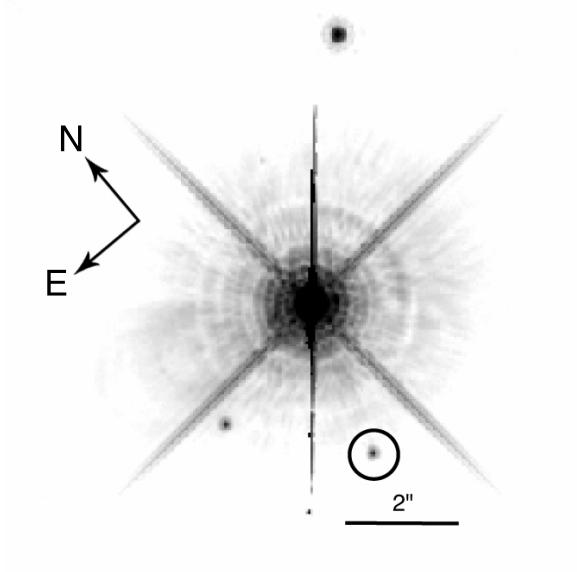


Figure 15. (left) The inner portion of the F845M WFC3 image of RV Sco. The possible companion is circled. A log scale is used, and $2''$ is indicated by the bar. (right) The CMD from the F845M and F621M WFC3 images for RV Sco. Symbols are the same as for Figure 10.

B. CANDIDATE COMPANIONS WITHIN $2''$: RESOLVED CLOSE COMPANIONS

The *HST* images for companion candidates within $2''$, discussed in Section 4.3.2, are presented in this Appendix both before and after PSF correction.

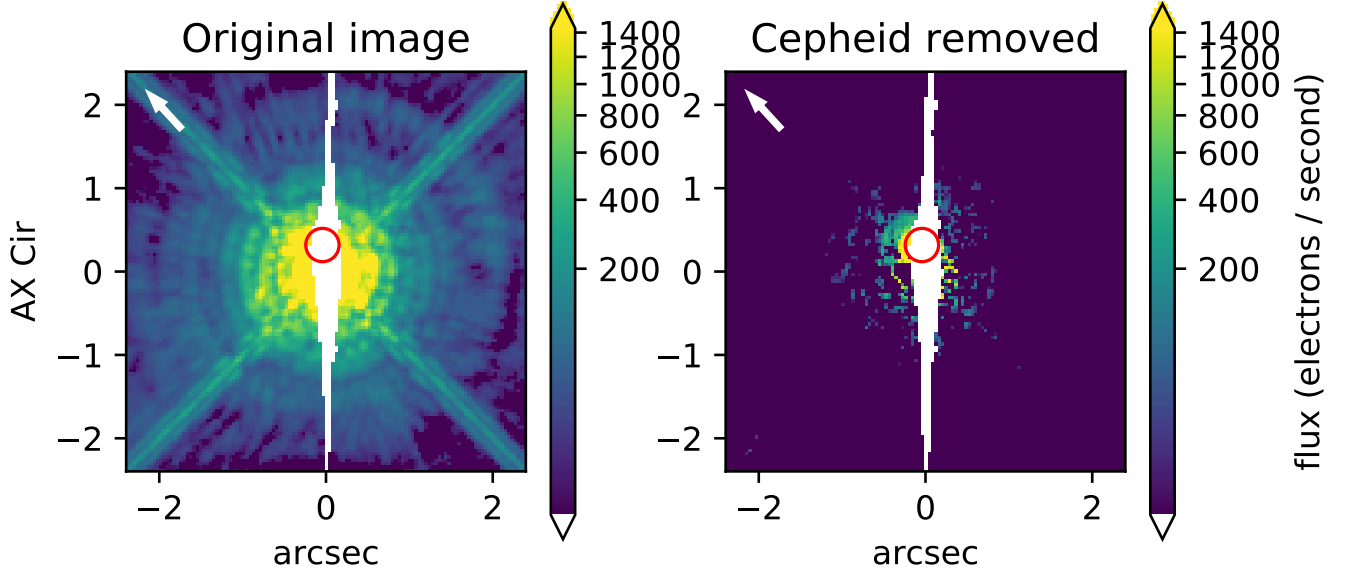


Figure 16. Image of AX Cir in the F845M band. The image is displayed in the same way as for Figure 3 (η Aql). Left: Original image. Right: after LOCI subtraction.

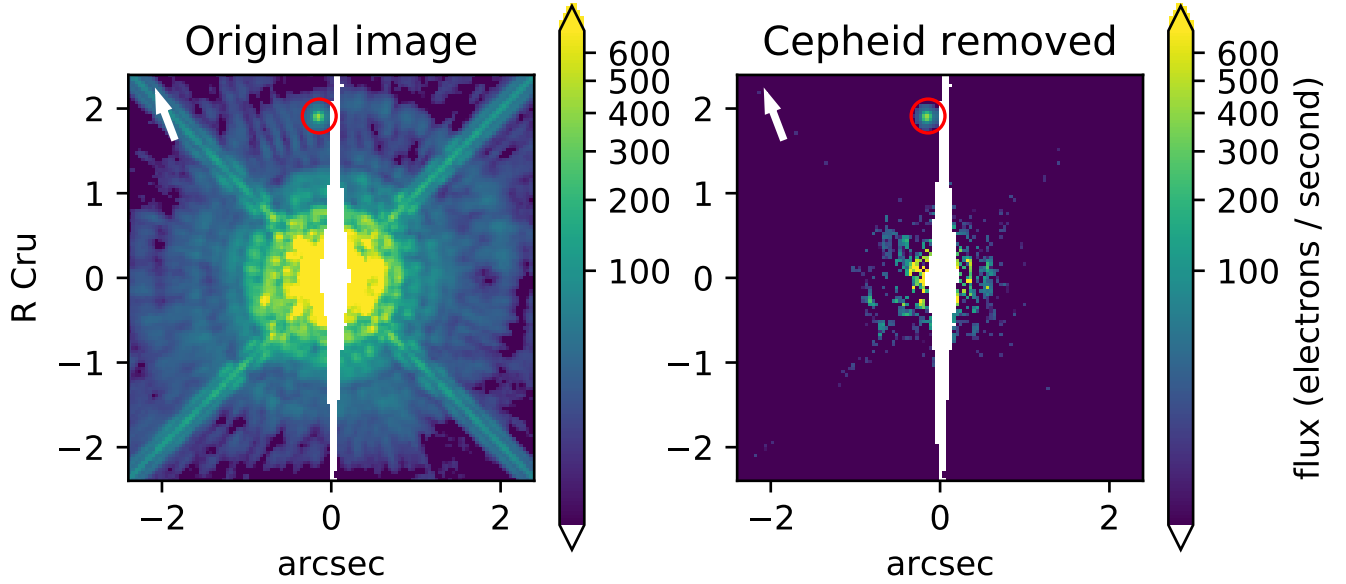


Figure 17. Image of R Cru in the F845M band. The image is displayed in the same way as for Figure 3 (η Aql). Left: Original image. Right: after LOCI subtraction.

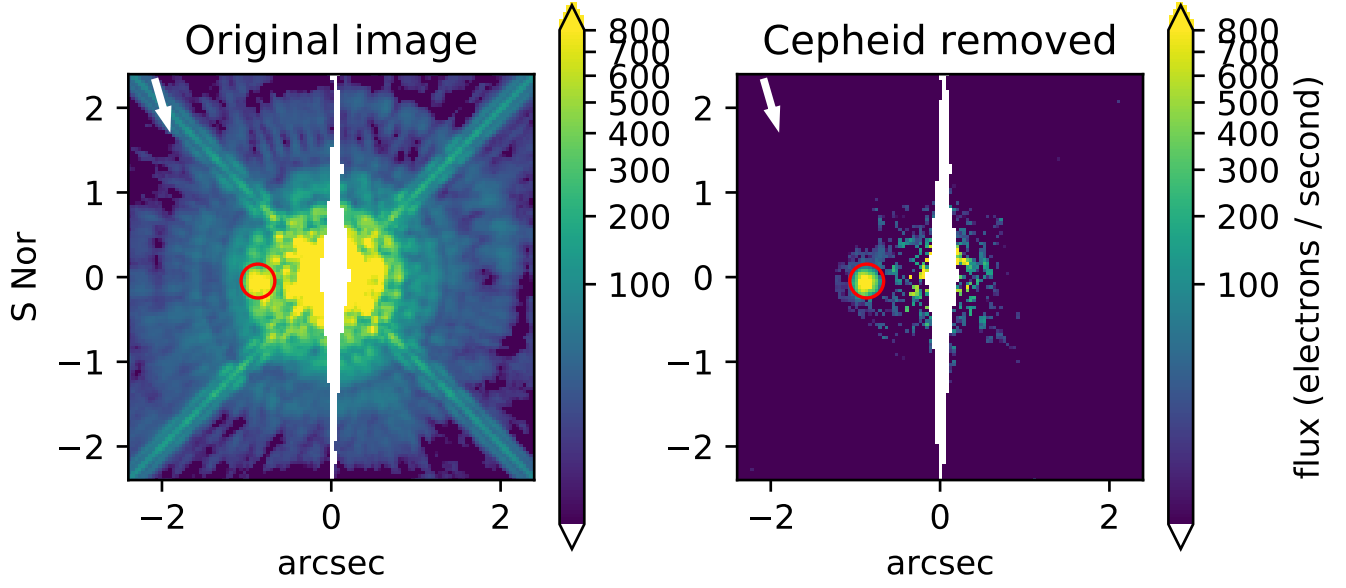


Figure 18. Image of S Nor in the F845M band. The image is displayed in the same way as for Figure 3 (η Aql). Left: Original image. Right: after LOCI subtraction.

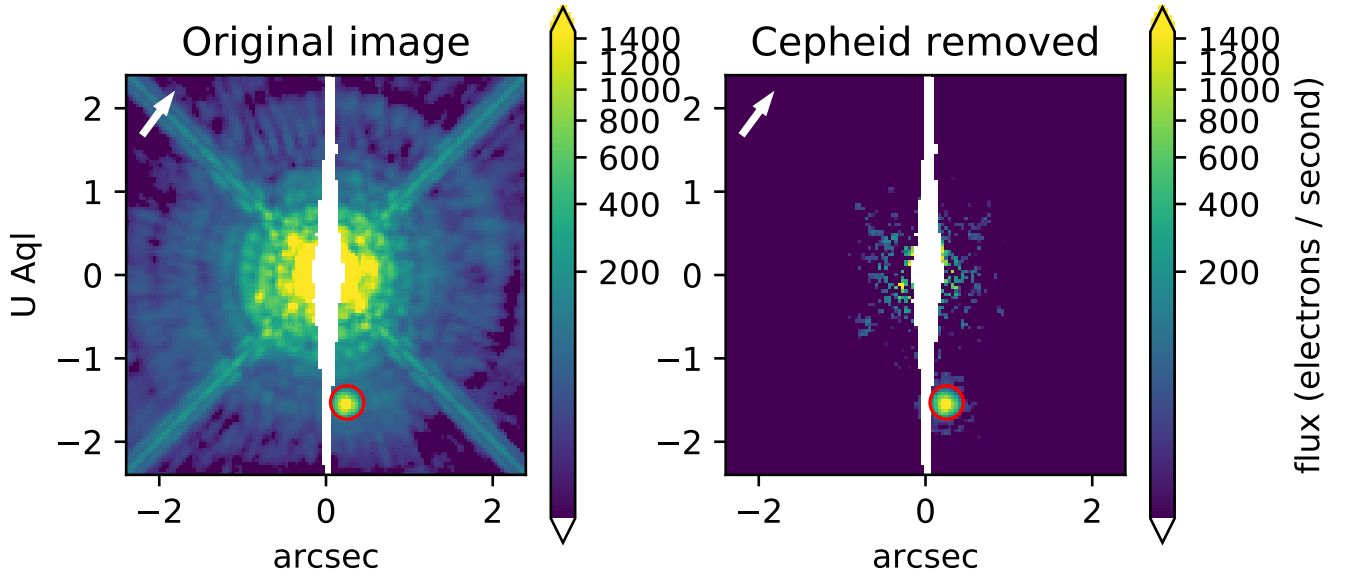


Figure 19. Image of U Aql in the F845M band. The image is displayed in the same way as for Figure 3 (η Aql). Left: Original image. Right: after LOCI subtraction.

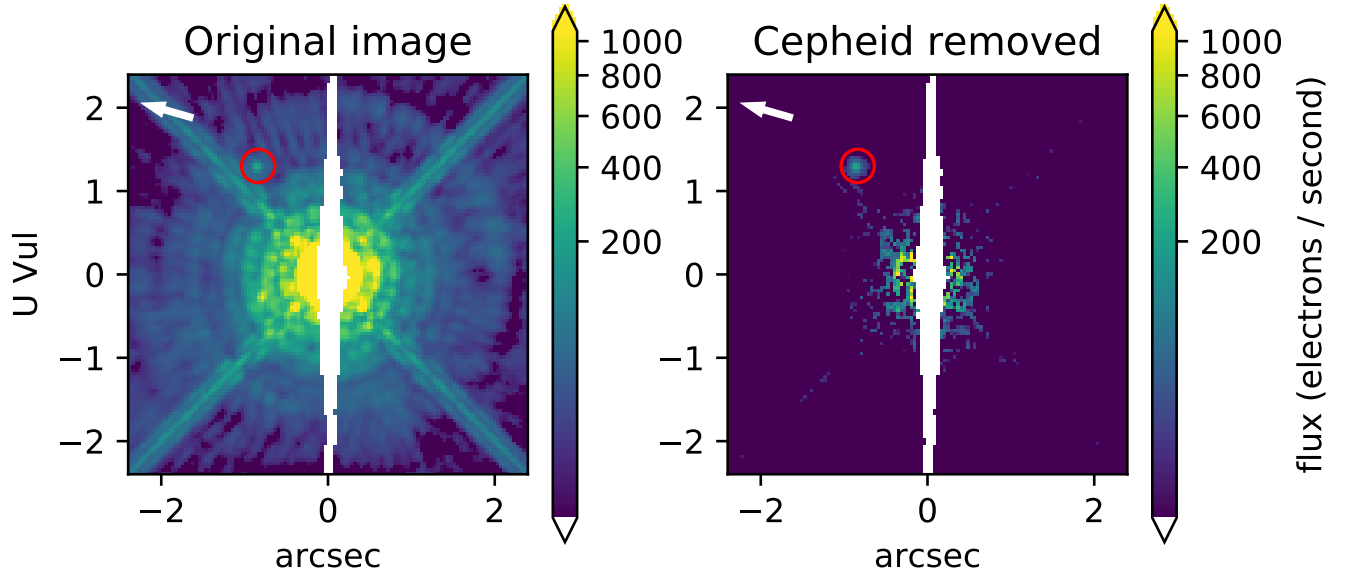


Figure 20. Image of U Vul in the F845M band. The image is displayed in the same way as for Figure 3 (η Aql). Left: Original image. Right: after LOCI subtraction.

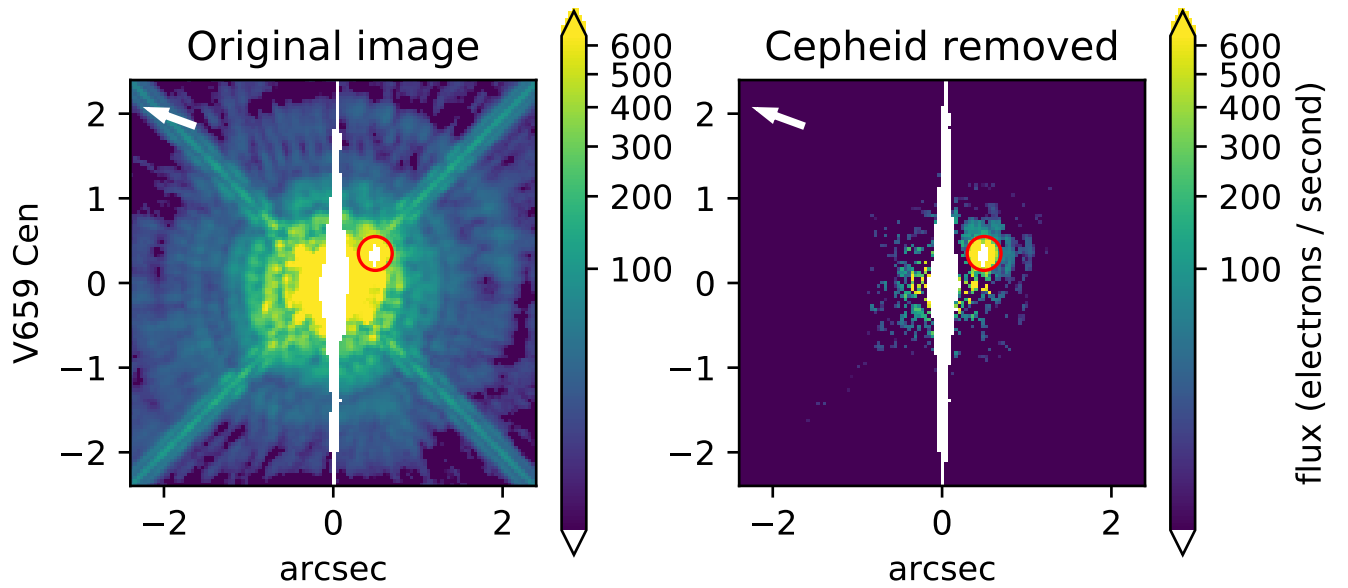


Figure 21. Image of V659 Cen in the F845M band. The image is displayed in the same way as for Figure 3 (η Aql). Left: Original image. Right: after LOCI subtraction.

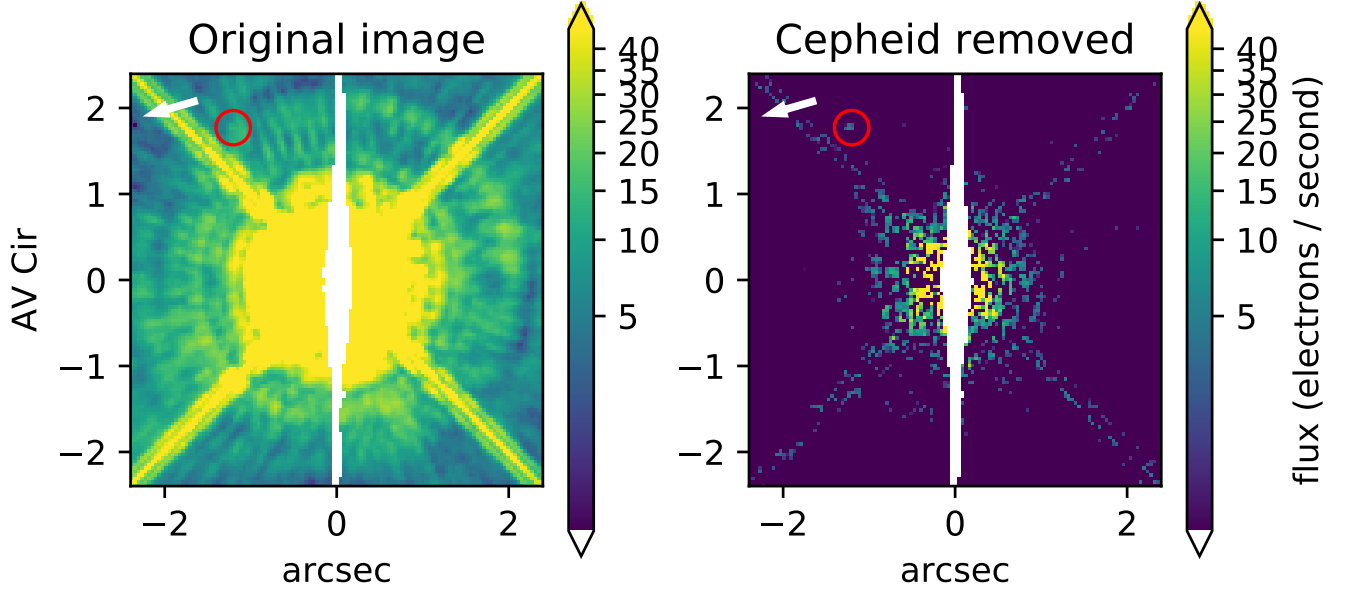


Figure 22. Image of AV Cir in the F845M band. The image is displayed in the same way as for Figure 3 (η Aql). Left: Original image. Right: after LOCI subtraction.

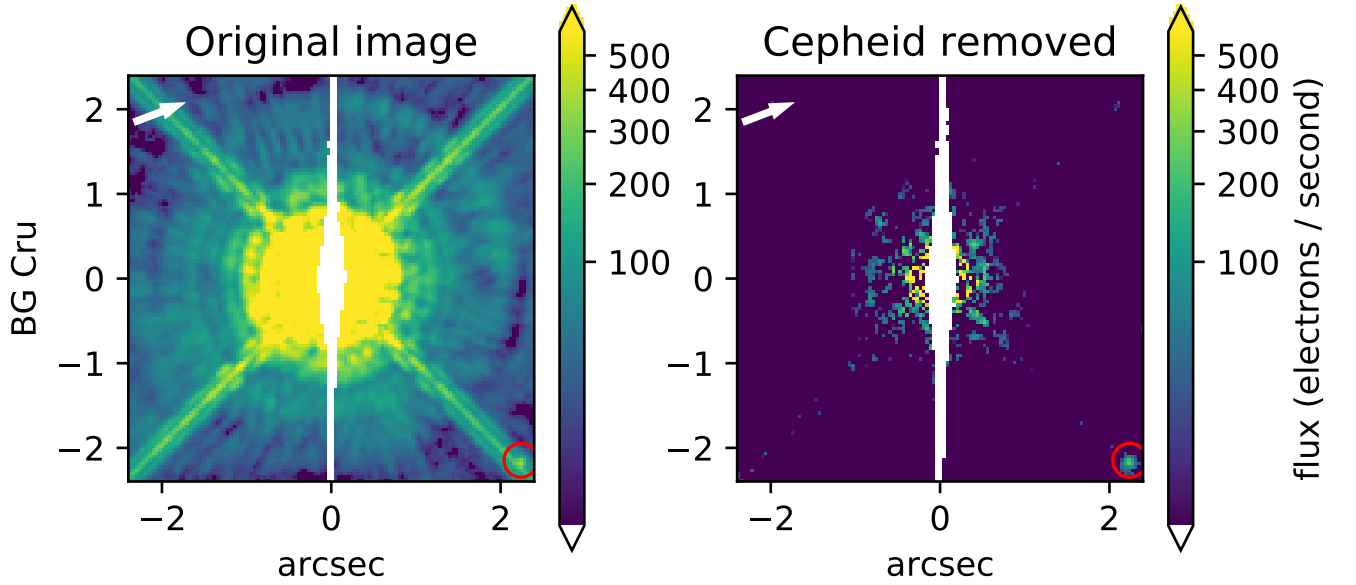


Figure 23. Image of BG Cru in the F845M band. The image is displayed in the same way as for Figure 3 (η Aql). Left: Original image. Right: after LOCI subtraction.

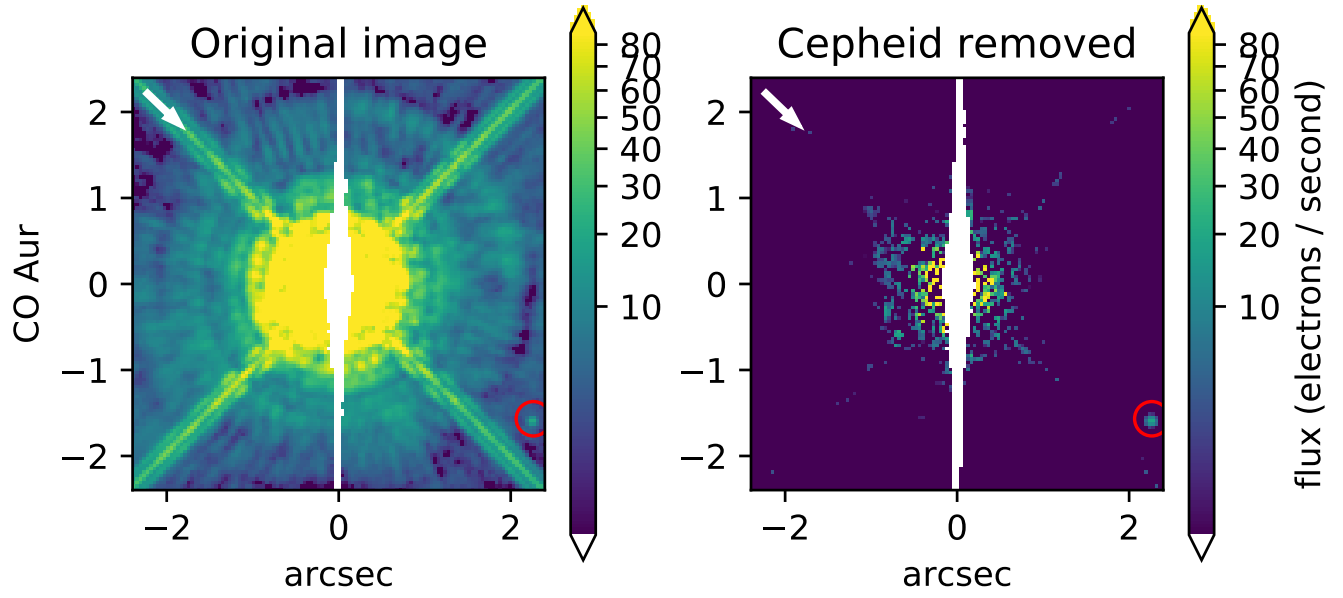


Figure 24. Image of CO Aur in the F845M band. The image is displayed in the same way as for Figure 3 (η Aql). Left: Original image. Right: after LOCI subtraction.

C. CHANDRA OBSERVATIONS

The goal of this paper is to identify resolved companions in the Cepheid *HST* snapshot survey and to examine the properties of members of the systems they belong to. As discussed in Paper IV, X-ray observations are an excellent way to distinguish between an X-ray-active star young enough to be a physical Cepheid companion, and an old field star without appreciable X-ray activity. Since Paper IV, we have added *Chandra* observations for two stars which add to the understanding of system parameters. The two systems were found to be X-ray sources in Paper IV: R Cru (Table 2) and S Mus. Among the *XMM* targets, they had X-ray detections at approximately the position of the Cepheid, but with a possible companion which was not resolved from the Cepheid in the *XMM* images. We followed up these detections with *Chandra* observations to identify the source of the X-rays, using the higher resolution of *Chandra*. S Mus and R Cru were observed with the Advanced CCD Imaging Spectrometer (ACIS) using the four “I” CCD chips. Details are provided in Table 12

Table 12. *Chandra* Observations

Star	OBSID	JD	Exp.
		−2,400,000	[ks]
S Mus	17740	57,388.068	5.0
R Cru	17741	57,578.170	14.9

C.1. *R Cru*

The *HST* and *XMM* images are shown in Figure 25, with the locations of the Cepheid and the possible optical companions circled. Either of the possible companions could be the source of the X-rays in the *XMM* image (although the closer one is more likely).

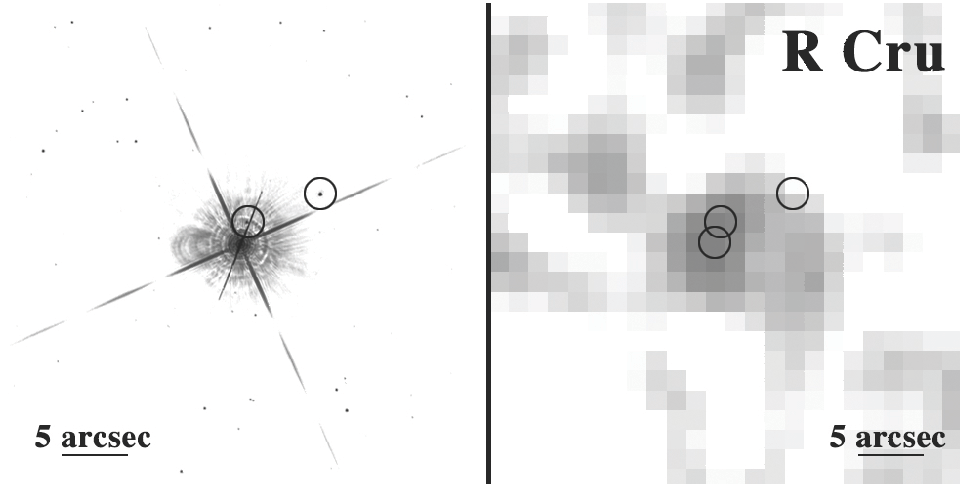


Figure 25. Possible companions of R Cru. Left: *HST* WFC3 *I*-band image of R Cru. Possible companions are circled. The stretch is logarithmic to emphasize faint features. Right: *XMM* image, again with circles indicating locations of the Cepheid and its two possible companions (including a small correction derived from the X-ray positions of 2MASS sources.) The orientation of both panels is the same: north up and east on the left.

The *Chandra* image of R Cru is shown in Figure 26, which compares the location of the X-ray source to that of the Cepheid and the possible close companion (including a small shift to align the Cepheid in the *HST* image with its coordinates from SIMBAD). The shape of the X-ray source based on a relatively weak detection has some uncertainty, but it is closer to the Cepheid than to the possible close companion.

Are the X-rays from the Cepheid itself? We now have a pattern to X-ray activity in Cepheids (Engle et al. 2017), that it is relatively constant at about $\log L_X = 28.8 \text{ ergs s}^{-1}$ for most of the pulsation cycle, but has a burst of X-rays just after maximum radius (approximately phase 0.5). The X-ray flux from *XMM* for R Cru ($\log L_X = 29.8 \text{ ergs s}^{-1}$; Paper IV) is larger than the quiescent level. The phase of the *Chandra* observation is 0.94 (using the period 5.825701^d and the epoch of maximum light of JD 2455172.5100 from Usenko et al. [2014]), not the phase of X-ray maximum. Thus the X-ray flux is larger than expected for the Cepheid, particularly at a phase other than maximum radius.

There is, however, another possibility. R Cru was observed with the CORAVEL radial-velocity spectrograph for 4 seasons, approximately 1996 July, and 1997 March, July, and December (Bersier 2002). The results are shown in Figure 27, with different symbols for each season. The velocities for the third season (and to some extent the fourth) fall below the first two, particularly considering that a typical error for the velocities is 0.33 km s^{-1} . This indicates a systemic velocity change within a year, presumably due to orbital motion. This implies that there is a second companion candidate in a close orbit, which would be unresolved from the Cepheid in the *Chandra* observation. An orbit with a period near a year corresponds to a separation near one AU.

There is one further piece of information which gives insight into the R Cru system. It was observed with *IUE* (Evans 1992a), with the result that any companion must have a later spectral type than A2, corresponding to a mass less than $2.5 M_\odot$.

To summarize companion possibilities for R Cru, there are two reasonably close companions, one at a separation of 1580 AU (Table 4), and the spectroscopic binary companion (Figure 27) at approximately 1 AU. Note that these two would be dynamically compatible. The *Chandra* observation in Figure 26 provides an indication favoring the closer companion, but this is tentative. However *Gaia* data (Kervella et al. 2019b) provide additional evidence that the candidate at 1580 AU is a physical companion, as discussed in Appendix D. Therefore we continue to include it in Table 4. The *IUE* observation shows that any companion is only about half as massive as the Cepheid (or less).

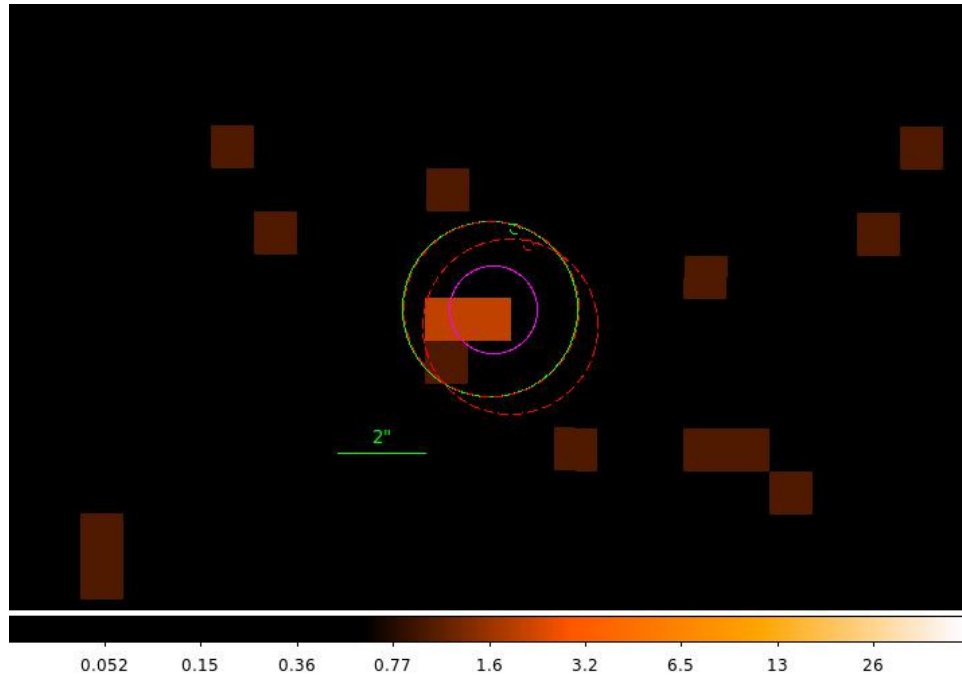


Figure 26. The center of the *Chandra* image of R Cru, showing the Cepheid and the closer companion. The orientation is the same as in Figure 25. The bright red rectangle is the location of the *Chandra* source. The circles are as follows: green: $2''$ radius centered on the position of the Cepheid from SIMBAD (including proper motion); red: the same radius centered on the Cepheid in the *HST* image; magenta: $1''$ radius within the green position of the Cepheid. The position of the companion from the *HST* image is shown by the very small red and green circles (about 1 o'clock) corresponding to the positions of the Cepheid in those colors. The image is a log stretch.

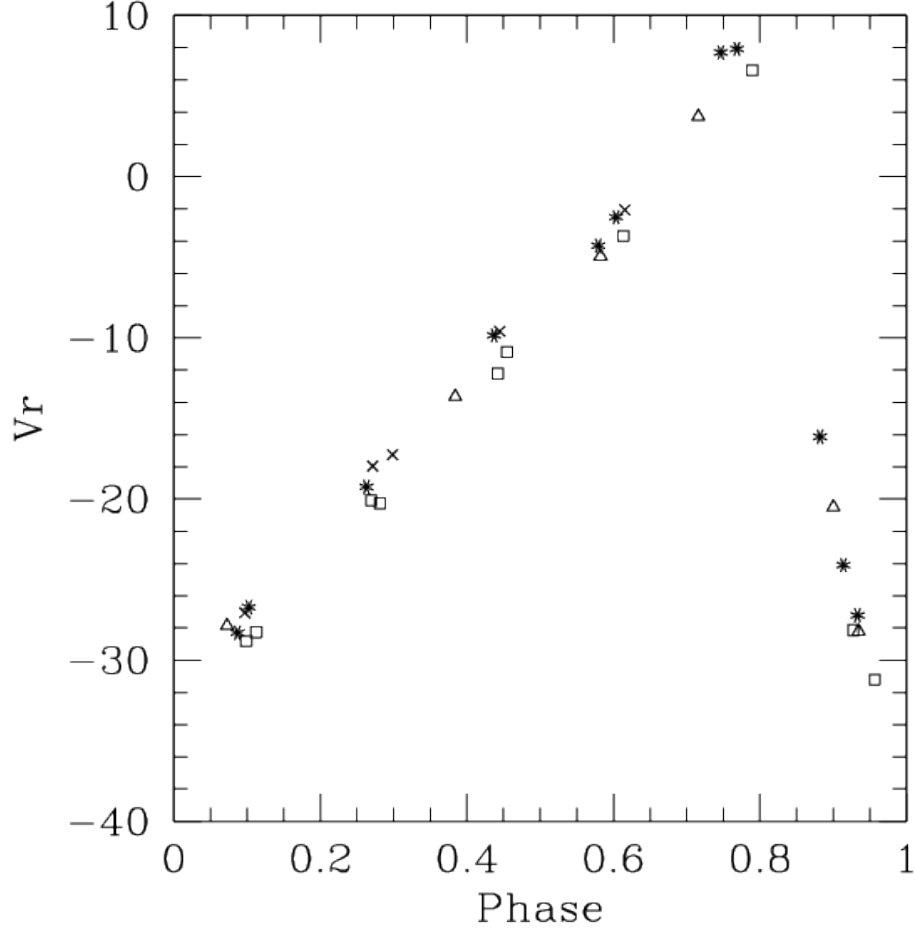


Figure 27. CORAVEL radial velocities of R Cru. The sequence of the four seasons of observations from first to last is: x's, asterisks, squares, and triangles (see text). The displacement of the squares from x's and asterisks is particularly apparent. Velocities are in km s^{-1} .

C.2. *S Mus*

The *HST* and *XMM* images are shown in Figure 28, with the locations of the Cepheid and the possible companion circled. Figure 29 shows the *Chandra* image with the same two locations overlaid. It has been mildly smoothed with the *CIAO* tool smooth.

The *Chandra* image rules out the $5''.2$ (4540 AU) companion as young, and hence it is not a physical companion of the Cepheid *S Mus*. The Cepheid is a member of a spectroscopic binary system with a period of 505 days ($a \sin i = 2.8$ AU; Paper I). The companion is the hottest known Cepheid companion: B3 V (Evans et al. 2006). Stars this hot produce X rays through wind shocks (Harnden et al. 1979), typically with $L_x/L_{\text{bol}} = 10^{-7}$. Using M_{bol} for a B3 star of -4.0 (Drilling & Landolt 2000), the luminosity is $1.2 \times 10^{37} \text{ ergs s}^{-1}$. Thus the X-ray luminosity of $\log L_X = 30.46$ (Paper IV) is close to the expected ratio for a hot star. The phase of the *Chandra* observation is 0.06, using the pulsation period and epoch of Petterson et al. (2004). Hence, *S Mus* is much brighter than the quiescent phases. Thus the flux must be at least heavily dominated by the hot companion.

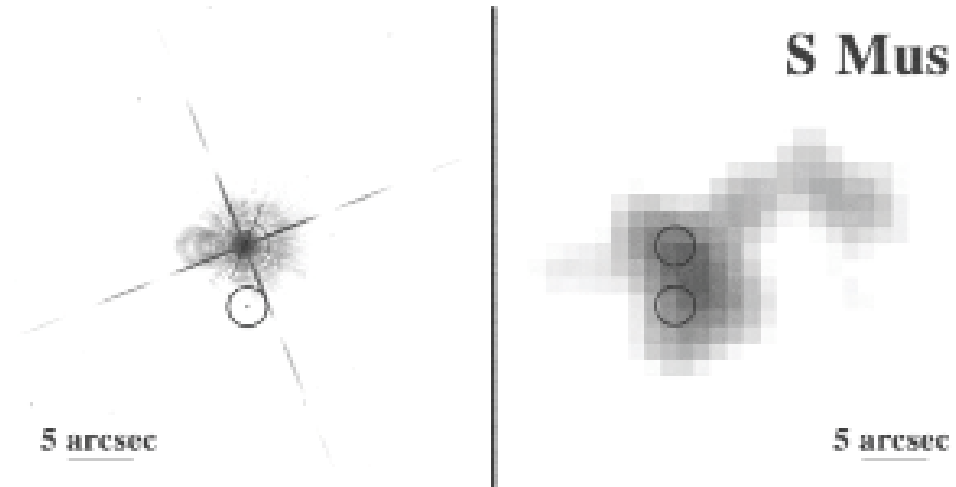


Figure 28. Possible companion of S Mus. Left: The *HST* WFC3 *I*-band image of S Mus. The possible companion is circled. The scale is logarithmic to emphasize faint features. Right: The *XMM* image, again with circles indicating the locations of the Cepheid and the possible companion (including a small correction derived from the X-ray positions of 2MASS sources.) The orientation of both figures is the same with N up and E on the left.

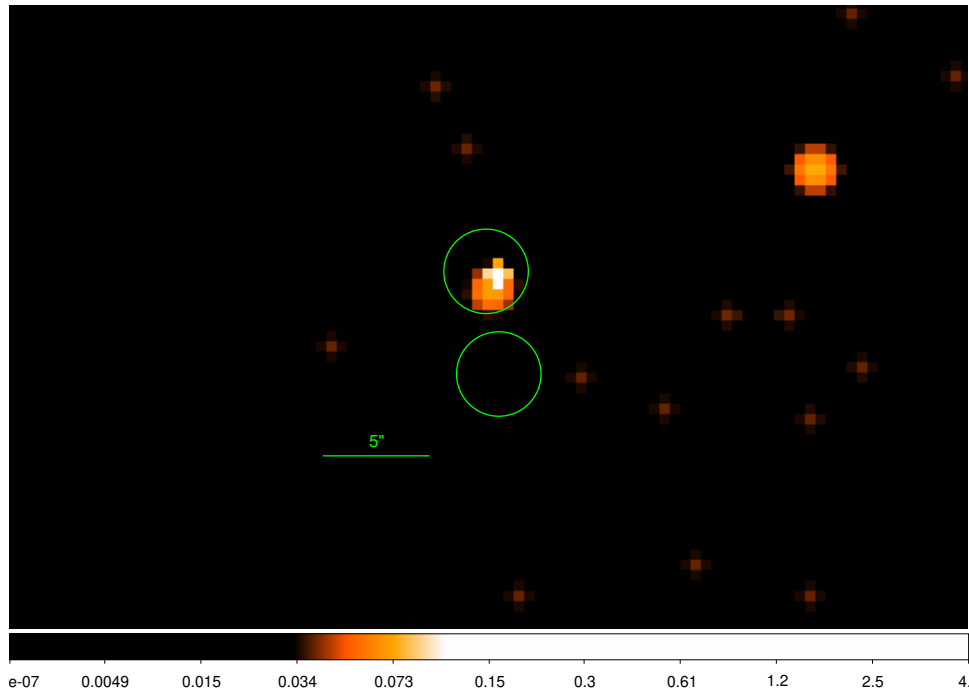


Figure 29. The center of the *Chandra* image of S Mus. The orientation is the same as Fig 28. The two circles (2'' radius) show the positions of the Cepheid and the possible companion in Fig 28. The image counts are on a log scale and have been mildly adaptively smoothed.

D. SYSTEMS WITH A RESOLVED COMPANION CLOSER THAN 2''

In this Appendix we discuss the components in systems with a resolved close companion. The results are summarized in Table 6.

S Nor: Although the companion is slightly closer than 1'', the photometry in Table 4 from the WFC3 images is used. From an *IUE* spectrum, Evans (1992b) found a B9.5 V companion, which has essentially the same M_V as in Table 3, implying that it is the resolved companion.

Are there any other components in the system besides the Cepheid and the resolved component? An inner binary in the S Nor system is likely but not proven. Mermilliod, Mayor, & Burki (1994) and Bersier et al. (2002) find little evidence of orbital motion in three well-covered seasons of CORAVEL data. Groenewegen (2008) found a low-amplitude orbit (2.53 km s^{-1}) with a period of 3584 days. However, the three seasons of CORAVEL data span 2700 days, so that orbital period seems unlikely (though not impossible). Gallenne et al. (2019) added radial-velocity data spanning 1700 days, but were unable to find an orbital signature. Kervella et al. (2019a) found differential proper motions between *Hipparcos* and *Gaia* marginally consistent with orbital motion. Combined with the orbit from Groenewegen, they found a companion mass of $1.5 M_\odot$, approximately an F0 V star. The orbit has a semimajor axis of 8.87 AU. Gallenne et al. (2019) observed the system with interferometry from the VLTI. If the hot star were the spectroscopic companion, it might have been marginally detectable but they found no detection at a level greater than 2.3σ . An F0 V star would not be expected to be detected. (The resolved companion in Table 2 is outside the field.) In summary, this confirms that the resolved companion is probably the one dominating the *IUE* spectrum. Estimated properties of the inner binary are in Table 6. Thus, there is evidence of a short-period binary; however an orbit is still uncertain, which may be due to a low-mass companion, the orbital inclination, or high eccentricity.

S Nor is a member of a cluster (NGC 6087) which may affect either the formation scenario or its dynamical history. One of the possible companions in our WFC3 survey is an X-ray source (Paper IV; Table 6), with a separation from the Cepheid of 15'' or 13,300 AU. The spectral type is derived from the $(V - I)_0$ color, using the calibration of Drilling & Landolt (2000). However, since it has an unusually large separation from the Cepheid (Figure 8), the conclusion in Paper IV was that it is likely to be a chance alignment with a cluster star, similar to the case of δ Cep. Kervella et al. (2019b) find additional companions at 41,100 and 38,800 AU (Table 9), and note that many stars have similar proper-motion vectors. They do not confirm the companion discussed by Evans & Udalski (1994) at a separation of 32,000 AU. The most likely companion properties for companions within 15'' are summarized in Table 6, although associated cluster members clearly complicate identification.

η Aql: Two companions to the Cepheid are known in this system. The companion in Table 5 is illustrated in Paper I and Figure 3. Gallenne et al. (2014a) used VLT/NACO to measure the properties of the companion at 0''.65, which they identify as an F1 V to F5 V star, corresponding to $(V - I)_0 = 0.37$ to 0.53 (Bessell & Brett 1988). They measure $H_0 = 9.34$. Using the calibration of Bessell and Brett, this corresponds to $V_0 = 10.1$ to 10.5. This is good agreement with a $V_0 = 10.0$ (Table 5), even at a separation of only 0''.6 from the Cepheid. At a distance of 273 pc, this corresponds to $M_V = +3.0$ to $+3.3$. In Tables 5 and 6 and Figures 6 and 7 we substitute the color $(V - I)_0 = 0.4$ and $M_V = +3.2$ for the contaminated color and magnitude in Table 2

There is a second, hotter companion detected in an *IUE* spectrum, with a spectral type of B9.8 V (Evans 1991). In Table 6 the V_0 and M_V are listed from that source. This second companion must be closer to the Cepheid and unresolved by either Gallenne et al. or in this study. However, neither it nor the Cepheid itself affect the measurement of companion in Table 4 using the resolved photometry of Gallenne et al. Unfortunately, *Gaia* data are poor for a star as bright as η Aql. Benedict et al. 2018 reported a preliminary orbit for the inner companion based on high precision radial velocities of η Aql. Additional radial velocities (Barnes et al. 2021 in preparation) have not confirmed that orbit as yet. We include in Table 6 a very preliminary value of the semimajor axis estimated from the masses, and a period of 4 years which can at least be used in the schematic distribution of separations. While orbital information is sketchy, there is no doubt that there is a third star in the system, and that it is closer to the Cepheid than the resolved companion in Table 4. Preliminary indications are that the orbit is nearly face-on and possibly eccentric.

V659 Cen: As can be seen from the discovery image (Paper I, Figure 1 and Figure 21), the companion in that image lies on a diffraction spike (in addition to being very close to the Cepheid), so the photometry is unreliable. However, there is information about the hottest companion from an *IUE* spectrum (Evans 1992b), in which the companion is found to be a B6.0 V star. This results in a corrected $E(B - V)$ for the Cepheid of 0.21 mag, and an absolute magnitude for the companion of -0.32 mag. A mild extrapolation from Table 15.11 of Drilling & Landolt (2000) provides $V - I = -0.16$.

The system was also resolved by *Hipparcos* (HIP 65970), with very similar parameters: PA 234° , separation $0''.574$.

To search for a possible inner companion, radial velocities were investigated. Possible orbital motion for V659 Cen must be small, and Lloyd Evans (1968) rated it as questionable at best. Lloyd Evans (1982) added new velocities to previous data, and concluded that the velocity differences between three seasons were probably not significant. However, R. I. Anderson (in preparation 2020) has identified orbital motion in a more recent series of observations. Kervella et al. (2019a) investigated *Gaia* DR2 and *Hipparcos* proper-motion anomalies as indications of orbital motion. They found marginal evidence in the *Hipparcos* data. In the *Gaia* data there is no significant anomaly, but the error in the proper-motion vector is unusually large, which could be due to orbital motion, particularly of a close companion. Based on this we have added a tentative entry in Table 6 and Figure 8 of 3 AU, reasonable for an orbit of a few years. Pending confirmation of orbital motion, V659 Cen would have both a resolved companion and a closer spectroscopic companion. Just prior to submission, we obtained an *HST* STIS G140L spectrum oriented to separate the resolved companion from the Cepheid. This spectrum shows that the resolved companion is the hottest star in the system, with the spectroscopic binary companion being much cooler. Entries in Table 5 are based on the *IUE* spectral type. Kervella et al. (2019b) find an additional very wide ($62''$) gravitationally bound low-mass (M3 V) companion.

AX Cir: This is the closest companion to a Cepheid identified here, and has particular problems for that reason. It is clear from the F845M image, however, that there is a star partly obscured by the bleed column and a diffraction spike. For this reason, the F621M filter is not usable, hence a color is not available. In the discussion below, we use the results from an *IUE* spectrum for further information about the companion.

The AX Cir system has been resolved 3 times: 2018 (Tokovinin et al. 2019), 1991.25 (HIP 72773), and 1913 by Innes.

AX Cir is also a member of a binary system (Petterson et al. 2004). An *IUE* spectrum shows that the hottest star in the system is a B6 V star (Evans 1994). The system was resolved with VLTI/PIONIER interferometry (Gallenne et al. 2014b) with a projected separation of 29.2 ± 0.2 mas, which corresponds to a separation of 15.4 AU at a distance of 527 pc. The separation of the wider companion ($0''.3$ in Table 4) corresponds to 158 AU. An *HST* STIS spectrum (Gallenne, Evans, Kervella et al. 2020 in preparation) showed that the B6 V star is the wider companion. From the STIS spectrum the spectral type of the close spectroscopic companion was found to be B9 V. A tentative velocity measure of the close companion from the STIS spectrum indicates that the most likely interpretation is that the inner companion is itself a short-period binary, making a total of four components in the system. Kervella et al. 2019a find a strong indication from *Gaia* and *Hipparcos* proper motions of an anomaly indicating a short-period orbit of the close companion. Combining this with the Petterson orbit and an estimated mass for the Cepheid, they find a companion mass larger than the Cepheid mass, confirming that the companion is itself a binary. Kervella et al. (2019b) also find a wider ($81''.5 = 43000$ AU) likely gravitationally bound system member, which is a low-mass M3.5 V star (Table 9). As with V659 Cen, we include the M_V and $(V - I)_0$ inferred from the *IUE* spectrum in Table 6

R Cru: There are three companion candidates to this system.

1. The M_V and $(V - I)_0$ in Table 5 correspond to an early K star. (The WFC3 photometry for a companion at this separation is much less likely to have contamination from the Cepheid than closer companions.)

2. To check for additional system members, radial velocities were investigated as discussed above. The orbital motion in Figure 27 partly guided by the position of the X-ray source (Appendix C) provides evidence for a companion inside the one identified in this study (Table 3). Kervella et al. (2019b) also find marginal evidence in *Gaia* and *Hipparcos* proper motions of short-period orbital motion, which would be consistent with the radial-velocity orbit. As a preliminary estimate of the separation for an inner companion, orbital motion within a year suggests a period of a couple of years. We have used this approximation to add this companion to Figure 8 and Table 6. We know from *IUE* observations (Evans 1992a) that the companion in the system is cooler than A2, corresponding to a mass of $2.7 M_\odot$.

3. We have also reinstated the $7''.6$ companion from Paper II for the following reasons. Kervella et al. (2019b) find that it is at the same distance as the Cepheid using *Gaia* data and is a gravitationally bound companion (spectral type G8 V). Possible orbital motion is detected. We note that there are X-ray counts from *XMM* in the position of that companion in Paper IV, although it is not the most prominent source in the field. The *Chandra* image (Figure 26) is a shallower image, hence this companion is not detected.

U Aql: In Appendix E there is extensive new material about U Aql, for which we provide a detailed discussion. There are three companions to the Cepheid in this system. M_V for the companions is from Table 13. The spectral type of the $1''.6$ companion is estimated to be A5 V from the STIS spectrum. We use the calibration of Drilling & Landolt

(2000) of $(V - I)_0 = 0.16$. This is in agreement with the value in Table 11 for a companion with a separation of $1''.6$. Component B (close) has an estimated projected separation of 66 AU and spectral type of A3-4 V (Appendix E).

The $1''.6$ pair of U Aql has been measured twelve times since the first resolution by Kuiper in 1934. It has always been at about the same relative position.

The U Aql spectroscopic binary was resolved at three epochs with the VLTI PIONIER combination (Gallenne et al. 2019). Using a distance of 592 ± 19 pc, they determined preliminary masses for the Cepheid and the spectroscopic companion of 6.2 ± 0.8 and $2.2 \pm 0.2 M_\odot$, respectively. This is somewhat smaller than the mass inferred from the B9.8 V spectral type using the Drilling & Landolt calibration. However it agrees with the Harmanec (1988) calibration within the errors (decreased by 0.02 in log M since the companions of Cepheids will be younger than average main-sequence stars of their spectral type [Evans et al. 2018]). A strong anomaly was detected in the *Gaia* and *Hipparcos* proper motions (Kervella et al. 2019a). The inferred separation and companion mass (assuming a Cepheid mass) are in agreement with those of Gallenne et al. (2019). The derived separation in Table 6 is the combined interferometric separation from Gallenne et al. and the distance from Paper II. No wider resolved companions were detected in the *Gaia* data (Kervella et al. 2019b).

U Vul: The M_V of the U Vul companion in Table 5 corresponds to a K0 star (Drilling & Landolt 2000). Another system member is indicated by an orbit for U Vul which was published by Imbert (1996), which has a high eccentricity and low amplitude. Kervella et al. (2019a) found a significant proper-motion anomaly in the *Gaia* and *Hipparcos* data. Assuming a Cepheid mass, they found a mass for the spectroscopic companion of $2.4 \pm 0.4 M_\odot$ and a semimajor axis of 7.1 AU. The upper limit of spectral type from an *IUE* spectrum is A1 V corresponding to a mass of $2.5 M_\odot$, which is in agreement with (and very close to) the Kervella mass within the errors. Note that this upper limit pertains to any companion in the system, both the spectroscopic companion and the resolved companion (Table 4). No wider resolved companions were found in the *Gaia* DR2 data (Kervella et al. 2018b).

E. U AQL

The quest for masses and luminosities for Cepheid variables has benefited greatly from the availability of the ultraviolet spectrum using satellites (*IUE* and *HST*). Through these studies, the picture of multiplicity has become increasingly complex. U Aql = HD 183344 is a good case in point. Its substantial orbital motion was only recognized in 1979 (Slovak et al. 1979). Welch et al. (1987) provide an orbit, as well as a summary of previous velocity information. The spectrum of the hottest star in the system dominates in the ultraviolet below about 2000 Å, and *IUE* observations have been discussed by Böhm-Vitense & Proffitt (1985) and Evans (1992). These provided a temperature of 9300 ± 100 K and a spectral type of B9.8 V respectively.

E.1. Companions

New insight into the system came with *HST* Faint Object Camera (FOC) and Space Telescope Imaging Spectrograph (STIS) images (PI: D. Massa). The STIS image was made with the G230L grating and the STIS NUV-MAMA detector. A series of spectra were taken at varying roll angles and times in the orbit. Similar data are fully discussed for AW Per (Massa and Evans 2008) and W Sgr (Evans, Massa, & Proffitt 2009). One of the images is presented as an example in Figure 30. Unexpected complexity in the system is immediately evident. The spectroscopic binary is the bottom spectrum, with the Cepheid Aa as the brightest star in the long-wavelength region and the companion Ab as the brightest star in the short wavelength region. At the top is the resolved companion C found in the *HST* WFC3 imaging (Table 2). Between them, but very close to the spectroscopic binary is a previously unsuspected companion B. The components are summarized in Table 6. In addition to the separation of C from Table 2, the projected separation of B has been measured from the STIS image. The separation in the spectroscopic binary Aa and Ab has been taken from the interferometry of Gallenne et al. (2019), 10.06 ± 0.16 mas. Using the distance from Paper II (613 pc), this becomes 6.2 AU.

Companion B may be the interferometric pair resolved three times by Ismailov (1992). However, it was not resolved by speckle at SOAR in 2008 and 2016 (Tokovinin et al. 2010 and 2018c respectively).

Spectra were extracted from the STIS image as described in Evans et al. (2009). The U Aql observations were done with the G230L and the unfiltered 25MAMA aperture. For the PSF comparison star we used the data set o6hr01040, an observation of the hot subdwarf GRW+70D5824. This exposure has relatively high S/N and was taken in February 2002, only a few months before the first of the U Aql observations. The image of U Aql which was analyzed was o6f101020, selected because it has the best projected separation between components. The projected

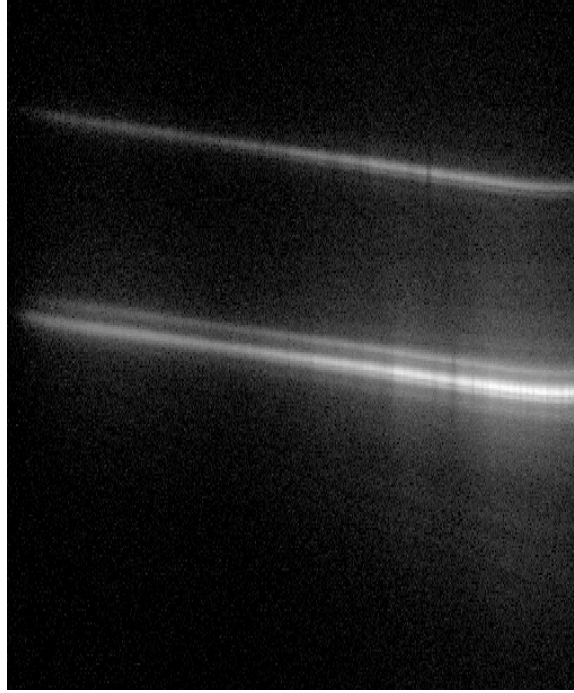


Figure 30. A flat-fielded image o6f101020 of the U Aql system. The wavelength increases to the right from about 1796 to 3382 Å. The lower component has the Cepheid (Aa; brightest at long wavelengths) and also the hottest star in the system (Ab; brightest at short wavelengths). The component at the top (C) is the one identified in the *HST* imaging (Table 2). A third component (B) is between them, close to the spectroscopic binary containing the Cepheid. The spectrum is on a log scale. The strongest feature in the Cepheid spectrum is 2800 Å.

separation between the spectroscopic binary with the Cepheid and the closest companion is $0.107''$ using a plate scale of $0.0247''/\text{px}$, which corresponds to 66 AU using the distance from Paper II. The results are shown in Figure 31. The Cepheid dominates in the long wavelength section, but the companions dominate at the short wavelength end. Components B and C are resolved and the Cepheid makes no contribution to the spectrum. For the spectroscopic binary Aa and Ab, however, in the region near 1800Å there is still a contribution from the Cepheid, although the companion Ab dominates. In this section we estimate the spectral types of all 3 companions, and we correct for the contribution of the Cepheid to the spectrum of Ab as follows. We use the *IUE* spectra of standard stars to create a spectrum B9.8 V (midway between B9.5 V and A0 V) as in Evans (1992b). (The B9.8 V spectrum has been reddened to match the U Aql spectrum and then scaled for comparison.) Figure 32 shows that the B9.8 V spectrum represents the U Aql companion Aa well at wavelengths shorter than 1500 Å, however the additional contribution from the Cepheid can be seen at longer wavelengths. Therefore we will use the flux from the B9.8 V spectrum to estimate the magnitude difference between the three companions in the U Aql system.

For all three companions in the U Aql system (Figure 33) the mean flux from 1650 to 1950 was created (Table 14) and from these the magnitude difference between the companions and the U Aql spectrum was created. At the bottom of Table 14 the fluxes from the *IUE* spectra are given. From the difference between the B9.8 V spectrum and the composite U Aql spectrum (Aa + Ab at 1800Å), a correction of 0.15 mag was derived to account for the contribution to the U Aql spectrum from the Cepheid. The far right column for the Far (C) and Close (B) companions from the STIS spectra includes this correction. Note that the *IUE* spectrum of the U Aql system includes all three companions although the hottest star in the system (Ab) is only affected in a minor way at the shortest wavelengths.

The spectral type of companion Aa was derived in Evans (1992b). To estimate the spectral type of the magnitude differences (Table 14), Table 15 shows the magnitude differences for main sequence spectral types from the *V*-ultraviolet colors (column 2) from Wesselius et al (1980) and the absolute magnitude calibration (column 3) from Drilling & Landolt (2000) for the ZAMS, which is essentially the same as used in Evans (1991, 1992b). The Far component C is approximately A5 V, and the Close component B is A3-4 V, corresponding to $M_V = +2.1$ and $+1.8$, respectively. This magnitude for C is very similar to that from the WFC3 value (Table 5).

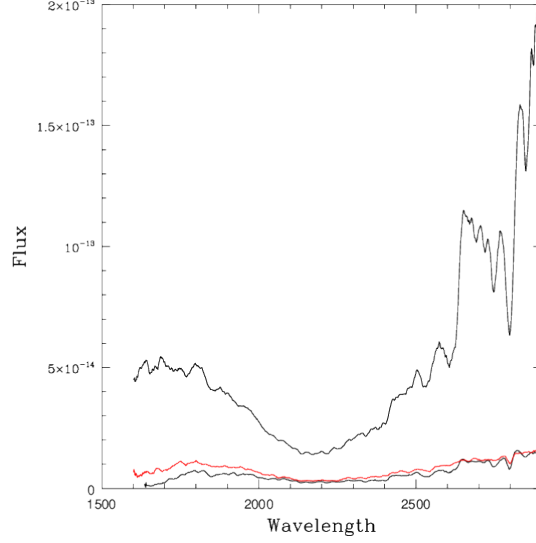


Figure 31. The extracted spectra for the U Aql system. The brightest spectrum is the spectroscopic binary containing the Cepheid and the hottest companion. The faintest spectrum is the wide companion. The spectrum in red is the close resolved companion.

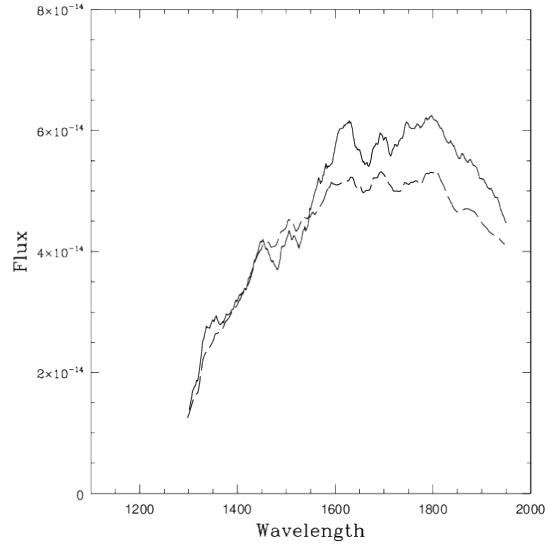


Figure 32. Comparison of the *IUE* spectra of U Aql and B9.8 V. The solid line is the U Aql spectrum; the dashed line is the B9.8 V spectrum.

E.2. Velocities

Previously Evans et al. (1998) obtained spectra with the Goddard High Resolution Spectrograph (GHRS) to measure the orbital velocity amplitude of the spectroscopic binary companion with the medium resolution grating G200M. The velocity difference between the two is -29.1 km s^{-1} with an estimated error of 3.8 km s^{-1} . Combining this with the orbital velocity amplitude of the Cepheid (Welch et al. 1987) and the mass of the main sequence companion they derived a mass for the Cepheid of $5.1 \pm 0.7 M_{\odot}$.

More recently, a spectrum was obtained with STIS. The spectrum used the E230H grating, and was taken over 2 days in 2003: August 1 (exposure time 12109 sec) and 14 hours later on August 2 (exposure time 7375 sec). Using the orbit of Welch et al. (1987) the orbital phase is 0.44. The data used are shown in Figure 34. A portion of the

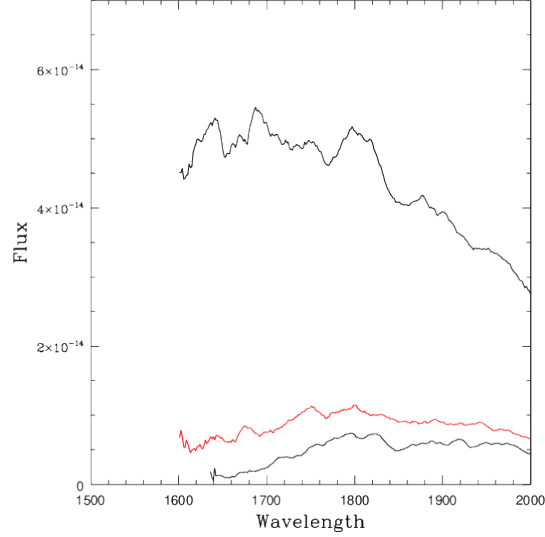


Figure 33. The three companions in the U Aql system in the short wavelength region. As in Figure 31, the spectrum in red is from the close resolved companion (B). The spectroscopic binary is represented by the B9.8 V spectrum.

Table 13. Components of the U Aql System

ID	Sep	Sep	M_V	SpTy
	"	AU	mag	
Ab	0.0101	6.2	1.2	B9.8 V
B	0.107	66	1.8	A3-4 V
C	1.6	981	2.1	A5 V

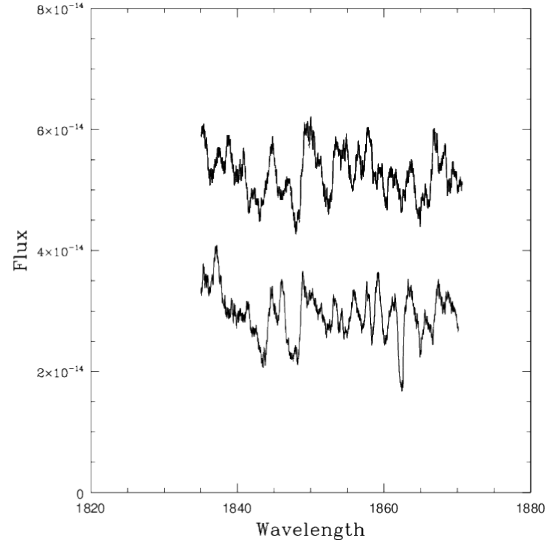
Table 14. Flux at 1800 Å

Star	f(1800)	$\Delta M(1800)$	Corr
	ergs cm ⁻² s ⁻¹ Å ⁻¹	wrt U Aql	
<i>HST/STIS</i>			
Far: C	5.01×10^{-15}	2.39	2.24
Close: B	9.14×10^{-15}	1.74	1.59
U Aql	4.52×10^{-14}		
<i>IUE</i>			
U Aql	5.64×10^{-14}		
B9.8 V	4.89×10^{-14}		

spectrum was selected where the blaze correction is satisfactory and there are spectral features. It was used in two ways. First the spectra for the two days were cross correlated to look for a velocity difference which could be caused by motion in a short period binary orbit. In addition the STIS spectrum was cross correlated with each of the GHRS spectra to confirm the orbital velocity amplitude in the 5 year orbit

Table 15. Energy Distributions of Companions

Spec. Type	M(1800 - V)	M_V	M(1800)	M - M(B9.8)(1800)
B9 V	-0.90	+0.9	+0.0	
B9.5 V	-0.70	+1.1	+0.4	
B9.8 V	-0.60	+1.2	+0.6	
A0 V	-0.51	+1.3	+0.8	0.2
A1 V	-0.21	+1.4	+1.2	0.6
A2 V	0.04	+1.5	+1.5	0.9
A3 V	0.27	+1.7	+2.0	1.4 B
A4 V	0.46	+1.9	+2.4	1.8 B
A5 V	0.68	+2.1	+2.8	2.2 C

**Figure 34.** The spectral region used in this analysis. The bottom is the spectrum from day 1 (see text); the top is the spectrum from day 2 shifted by 0.2×10^{-14} in flux for clarity. Both spectra have been smoothed by 100 points.

Although the spectrum on each day was weak, cross correlation of these two spectra provided the opportunity to check for possible orbital motion from a short period binary. The spectral lines are reasonably broad, which is not surprising for a late B main sequence star, resulting in a broad velocity peak. However Figure 35 shows no evidence of a change in velocity which would be an indication of short term binary motion.

This is in agreement with the mass of the secondary in Kervella et al. (2019a) incorporating *Gaia* and *Hipparcos* proper motions with the orbit. The mass is appropriate for a B9.8 V star, and would not accommodate an additional star.

To check the result from the two GHRS spectra (Evans et al. 1998), the STIS spectrum was cross correlated with each of the GHRS spectra. The result (Figure 36) showed a similar shift between the two orbital phases to that found previously. On the other hand, it is possible that the STIS spectrum is as much as 30 km s^{-1} smaller than both the GHRS spectra. In particular, the STIS spectrum should have a very similar orbital velocity to GHRS Visit 1.

In summary, the STIS spectra taken a day apart do not show any velocity signal that the companion is a very short-period binary. Comparison of the STIS and GHRS velocities (Figure 36) leaves open the possibility of a longer period binary with smaller orbital velocity. However, because of the broad lines, and hence the broad correlation, this is only a possibility.

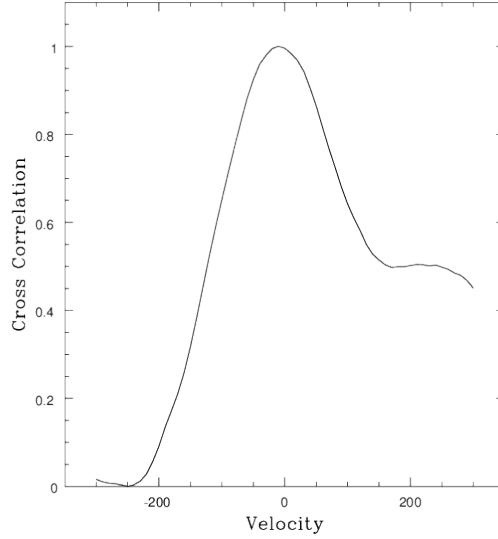


Figure 35. The cross correlation between the exposures on the day 1 and day 2.

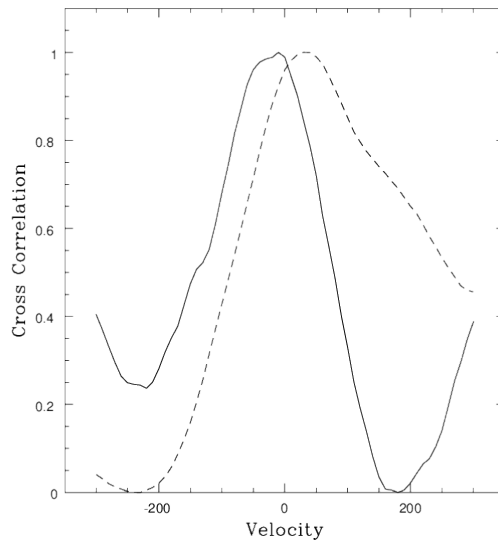


Figure 36. The cross correlation of the STIS spectrum with the two GHRS spectra. Solid line: the velocity of the GHRS Visit 1 spectrum with respect to the STIS spectrum; dashed line: GHRS Visit 2 with respect to STIS. The program returns velocities that are in the sense that the velocity of the companion has increased between Visit 1 and Visit 2.

E.3. Discussion

The STIS image (Figure 30) provides an explanation for a surprisingly large discrepancy between an absolute magnitude for the Cepheid from the *IUE* spectrum of the companion and the Leavitt Law (Period-Luminosity relation) of Feast and Walker (1987). As discussed in Evans (1992b) typical differences between the *IUE* absolute magnitudes and those of Feast and Walker are 0.2 mag for well exposed companion spectra with well known reddening. For U Aql the difference was more than twice that, even though both conditions were met. However, the addition of the flux from the two additional companions which were unknown at the time (but would have been in the *IUE* aperture) accounts for the discrepancy.

F. COMPANIONS IN SYSTEMS WITH A RESOLVED WIDE COMPANION (WIDER THAN 2'')

In this Appendix we discuss the components in systems with a resolved wide companion. The results are summarized in Table 7.

FF Aql: The interpretation of the companion in Table 4 from the ground has been “challenging”. Udalski and Evans (1993) concluded that it is not a physical companion. However the WFC3 measures (Paper II) found the photometry consistent with a physical companion. The Washington Double Star Catalog (WDS) finds no relative motion between the companion and Cepheid, indicating that they are moving together. In the recent discussion of *Gaia* DR2 data Kervella et al. (2019b) find that the parallax of the companion is consistent with that of the Cepheid, but that the proper motion has a projected relative velocity between the two of $\simeq 30 \text{ km s}^{-1}$. However, they describe the position and parallax of the two stars as “quite remarkable from a statistical point of view”, and suggest that binary motion in the companion is a possible explanation. FF Aql is a well known spectroscopic binary. Astrometric motion has been detected by Benedict, et al. (2007). It has been tentatively resolved by CHARA MIRC (Gallenne et al. 2019), with a separation of 8.9 mas. It also has strong indication of orbital motion in *Hipparcos-Gaia* proper motions (Kervella et al. 2019a). Combining proper motion information with the orbit, the separation (8.2 mas corresponding to 4.5 AU) and mass of the companion ($0.8 \pm 0.1 M_{\odot}$) were derived (Kervella et al. 2019; in Table 7). This corresponds to a spectral type approximately K0 V, which is later than the range estimated from *IUE* spectra (Evans et al. 1990). At present the inferred masses from Benedict, et al., Kervella, et al., and Evans et al. are not consistent, however improvement from the next *Gaia* release should resolve this. Kervella et al. (2019b) do not find likely wider companions.

RV Sco: *Hipparcos-Gaia* proper motions clearly show orbital motion (Kervella et al. 2019a), as was suspected by Szabados (1989), identifying a spectroscopic binary. As a very preliminary estimate of the separation (for plotting purposes), we use estimated orbital period of 8000^d, corresponding to a semimajor axis of 14 AU for reasonable masses. WDS measures for RV Sco indicate that the brighter resolved candidate at a separation of 6.0'' has no relative motion with the Cepheid, and hence is likely bound, making three components in the system. However, it is dynamically unlikely that both possible companions in Table 4 are bound, hence the 6.0'' is the most likely physical companion. An *IUE* observation of the system showed that all stars in the system are A3 V or later, corresponding to a mass of $1.9 M_{\odot}$ or less.

AP Sgr: *Hipparcos-Gaia* proper motions show weak indication of orbital motion (Kervella et al. (2019a). Radial velocity observations indicate possible low amplitude orbital variation (Gieren 1982; Lloyd Evans 1982; Szabados 1989), with a period estimate of 7000 days. As with RV Sco, this has been used to derive a very preliminary estimate of the semimajor axis in Table 7. Additional velocity observations are needed to confirm this. This would continue the pattern of an interior orbit found in systems with resolved companions. Alternately, the separation of the resolved companion is the second largest in Table 4, and the color of the companion is the reddest. This would be consistent with the companion being a line of sight coincidence with a field star. An *IUE* observation shows that any companion in the system is A5 V or later, corresponding to a mass of $\leq 1.8 M_{\odot}$. Two wider possibly comoving candidates (49,000 and 28,200 AU) have been identified by Kervella et al. (2019b). However, even the brightest (49,000 AU) is cooler than even a late M main sequence star. Both are fainter and cooler than the limit for our survey (hotter than M0 stars), so they are not included in Table 10.

BB Sgr: As with AP Sgr, there is some indication of low level orbital velocity (Gieren 1982; Barnes et al. 1988; Szabados 1989), but it is not conclusive. Velocities are available from Gorynya et al. (1996, 1998) from 1994 to 1997. As discussed by Evans et al. (2015), they have a γ velocity of 6.6 km s^{-1} , which is very similar to velocities assembled in Szabados (1989). Furthermore, there is no orbital motion to within less than 1 km s^{-1} in the Gorynya et al. data. Anderson (2020, in prep.) also sees no orbital motion. *Hipparcos-Gaia* proper motions show no anomaly consistent with orbital motion (Kervella et al. 2019a). An *IUE* observation shows that any companion in the system is A0 V or later, corresponding to a mass of $\leq 2.1 M_{\odot}$. BB Sgr is a member of the open cluster Collinder 394 (Anderson et al. 2013) As with S Nor this makes possible a line-of-sight coincidence with a cluster member, rather than a bound companion.

Y Car: Table 4 has two possible companions for Y Car, with similar separations from the Cepheid, but it is dynamically unlikely that both are bound companions. At larger separations, Kervella et al. (2019b) identify several stars with similar proper motions from *Gaia*, indicating that there may be a comoving group, making a chance line of sight alignment rather than a gravitationally bound companion likely for at least one of the candidates Table 7. Y Car is a well-known spectroscopic binary (Pettersen et al. 2004). A velocity from *HST* STIS spectrum of the companion indicated that the companion is itself a binary (Evans et al. 2005). The spectral type and mass of the hottest star in

the system was determined from an *IUE* spectrum to be B9.0 V and $2.4 M_{\odot}$. Preliminary estimates of the inclination and mass of the companion using *Hipparcos-Gaia* proper motions (Kervella et al. 2019a) provide a total mass of the two companion stars of $2.8 \pm 0.4 M_{\odot}$. (This is an estimate because the orbital period is relatively short, although there is a highly significant detection of orbital motion.) Since this is only slightly larger than the mass of the hotter star of the pair from the *IUE* spectrum, this implies that the second star in the companion pair has a low mass. The spectroscopic system with the Cepheid has been tentatively resolved (Gallenne et al. 2019) with the VLTI PIONIER, with a separation of 2.5 mas, corresponding to 3.6 AU. Table 7 summarizes the component properties considered most probable.

V350 Sgr: There is one possible resolved companion to V350 Sgr in Table 4. V350 Sgr is a well known binary system, where the mass of the Cepheid has been measured (Evans et al. 2018). The mass of $5.2 \pm 0.3 M_{\odot}$ comes from combining the ground-based orbit of the Cepheid with the orbital velocity amplitude of the companion from *HST* STIS spectra, and the mass of the companion inferred from *IUE* spectra of $2.5 M_{\odot}$. The mass of the companion determined from the spectroscopic orbit and the *Hipparcos-Gaia* proper motions is approximately 2σ from this: $3.4 \pm 0.5 M_{\odot}$ (Kervella et al. 2019b using the orbit derived by Gallenne et al. 2019). The proper motions have a strong orbital signature. A tentative resolution of the system was made with VLTI PIONIER (Gallenne et al. 2019) with a separation of 3.0 mas or 2.7 AU. Outside the *HST* survey here, which includes $20''$ around the Cepheid, two candidate bound companions are found from proper motion agreement (Kervella et al. 2019b), making it possible that the Cepheid is part of a 4 or 5 member system.

REFERENCES

- Anderson, R. I., Eyer, L., & Mowlavi, N. 2013, MNRAS, 434, 2238
- Anderson, R. I., & Riess, A. G. 2018, ApJ, 861, 36
- The Astropy Collaboration 2013, A&A, 558, 33A
- Barnes, T. G., Moffett, T. J., & Slovak, M. H. 1988, ApJS, 66, 43
- Benedict, G. F. et al. 2007, AJ, 133, 1810
- Benedict, G. F., Barnes, T. G., Evans, N. R., et al. 2018, AAS, 23110905B
- Bersier, D. Burki, G., Mayor, M., & Duquenoy, A. 2002, A&ApS, 108, 25 2002,
- Bersier, D. 2002, ApJS, 140, 465
- Bessell, M. S. 1979, PASP, 91, 589
- Bessell, M. S. and Brett, J. M. 1988, PASP, 100, 1134
- Böhm-Vitense, E. and Proffitt, C. 1985, ApJ, 296, 175
- Bradley, L. et al. 2019, zenodo, 3568287B
- de Mink, D. E., Sana, H., Langer, N., Izzard, R. G., and Schneider, F. R. N. 2014, ApJ, 782, 7
- Deacon, N. R. and Kraus, A. L. 2020, MNRAS arXiv 2006.06679
- Doe et al. 2007, ASPC, 376, 543
- Drilling, J. S., & Landolt, A. U. 2000, in Cox, A. N. *Astrophysical Quantities*, Springer: New York, p 381
- Duchêne, G. and Kraus, A. 2013, ARA&A, 51, 269
- Engle, S. G., Guinan, E. F., Harper, G. M., Cuntz, M., Evans, N. R., Neilson, H. R., and Fawzy, D. E. 2017, ApJ, 838, 67
- Evans, D. W. et al. 2018, A&A, 616, A4
- Evans, N. R., Welch, D. L., Scarfe, C. D., and Teays, T. J. 1990, AJ, 99, 1598
- Evans, N. R. 1991, ApJ, 372, 597
- Evans, N. R. 1992b, ApJ, 389, 657
- Evans, N. R. 1992a, ApJ, 384, 220
- Evans, N. R. 1994, ApJ, 436, 273
- Evans, N. R. and Udalski, A. 1994 AJ, 108, 653
- Evans, N. R., Böhm-Vitense, E., Carpenter, K., Beck-Winchatz, B., and Robinson, R. 1998, ApJ, 494, 768
- Evans, N. R., Carpenter, K. G., Robinson, R., Kiezle, F., and Dekas, A. E. 2005, AJ, 130, 789
- Evans, N. R., Massa, D., Fullerton, A., Sonneborn, G. and Iping, R. 2006, ApJ, 647, 1387
- Evans, N. R., Massa, D., and Proffitt, C. 2009, AJ, 137, 3700
- Evans, N. R., Bond, H. E., Schaefer, G. H., Mason, B. D., Karovska, M., and Tingle, E. 2013, AJ, 146, 93 (Paper I)
- Evans, N. R., Berdnikov, L., Lauer, J. et al. 2015 AJ, 150, 13
- Evans, N. R., Bond, H. E., Schaefer, G. H., Mason, B. D., Tingle, E., Karovska, M., and Pillitteri, I. 2016a, AJ, 151, 129 (Paper II)
- Evans, N. R., Pillitteri, I., Wolk, S., Karovska, M., Tingle, E., Guinan, E., Engle, S., Bond, H. E., Schaefer, G. H., and Mason, B. D., 2016b, AJ, 151, 108 (Paper IV)
- Evans, N. R., Proffitt, C., Carpenter, K. G., Winston, E. M., Kober, G. V., Guenther, H. M., Gorynya, N., Rastorguev, A., and Inno, L. 2018, ApJ, 866, 30
- Evans, N. R., Proffitt, C., Carpenter, K. C. et al. 2018, ApJ, 866, 30
- Feast, M W. and Walker, A. R. 1987, ARA&A, 25, 345
- Freeman et al. 2001, ASPC, 238, 48
- Gaia Collaboration, Prusti, T., et al. 2016, A&A, 595, A1
- Gaia Collaboration, Brown, A. G. A., et al. 2018 A&A, 616, A1
- Gallenne, A., Kervella, P., Merand, A., Evans, N. R., Girard, J. H. V., Gieren, W., and Pietrzynski, G. 2014a, A&A, 567, A60
- Gallenne, A., Mérand, A., Kervella, P. et al. 2014b, A&A, 561, L3
- Gallenne, A., Kervella, P., Evans, N. R., Proffitt, C. et al. 2020 in preparation
- Gallenne, A., Kervella, P. Borgniet, S. et al. 2019 A&A, 622, A164
- Gieren, W. 1982, ApJS, 49, 1
- Gilliland, R. et al. 2010, Inst Sci Rep WFC3
- Gorynya, N. A., Rastorguev, A. S., and Samus, N. N. 1996, AstL, 22, 175
- Gorynya, N. A.; Samus', N. N.; Sachkov, M. E.; Rastorguev, A. S.; Glushkova, E. V.; Antipin, S. V. 1998, AstL, 24, 815
- Groenewegen, M. A. T. 2008, A&Ap, 288, 25
- Hack, W., Dencheva, N., and Fruchter, A. S. 2013, ASPC, 475, 49
- Harmanec, P 1988, Bull Ast. Inst Czech, 39, 329
- Harnden, F. R., et al. 1979, ApJ, 234, L51
- Imbert, M. 1996, A&AS, 116, 497
- Ismailov, R. M. 1992, A&AS 96, 375
- Kervella, P. Gallenne, A., Evans, N. R., et al. 2019a, A&A, 623, A116
- Kervella, P., Gallenne, A., Evans, N. R. et al. 2019b, A&A, 623, A117
- Kroupa, 1995, MNRAS, 227, 1491
- Kuiper, G. 1934, PASP 46, 188
- Lafrenière, et al. 2007, ApJ, 660, 770
- Lloyd Evans, T. 1968, MNRAS, 141, 109
- Lloyd Evans, T. 1982, MNRAS, 199, 925
- Marois, et al. 2014, SPIE, 9148E, 0

- Massa, D., and Evans, N. R. 2008, MNRAS, 383, 139
- Mermilliod, J. C., Mayor, M., and Burki, G. 1987, A&ApS, 70, 389
- Moe, M. and Di Stefano, R. 2017, ApJS, 230, 15
- Moe, M. and Kratter, K. M. 2018, ApJ, 854, 44
- Naoz, S. 2016, ARAp, 54, 411
- Pecaut, M. J. and Mamajek, E. E. 2013, ApJS, 208, 9
- Petterson, O. L., Cottrell, P. L., and Albrow, M. D. 2004, MNRAS, 350, 95
- Reipurth, B. and Mikkola, S. 2012, Nature, 492, 221
- Sana, H. 2017, IAU Symp 329, 110
- Sana, H. de Mink, S. E., de Koter, A. et al. 2012, Sci 337, 444
- Sana et al. 2014, ApJS, 215, 15
- Slovak, M. H., Van Citters, G. W., and Barnes, T. G. 1979, PASP, 91, 840.
- Soummer, R. et al. 2012, ApJ, 755, 28S
- Stetson, P. 1987, PASP, 99, 191S
- Szabados, L. 1989, Mitt Stern Ungarischen Akad Wissen 94, 1
- Szabados, L. Anderson, R. I., Derekas, A. et al. 2013, MNRAS, 434, 870
- Tody, D. 1986, SPIE, 627, 733
- Tody, D. 1993, ASPC, 55, 173
- Tokovinin, A. et al. 2010, AJ 139, 743
- Tokovinin, A. 2017, MNRAS, 468, 3461
- Tokovinin, A. 2018a, AJ, 155, 160
- Tokovinin, A. 2018b, ApJS, 235, 6
- Tokovinin, A. et al. 2018c, AJ 155, 235
- Tokovinin, A, et al. 2019, AJ, 158, 48
- Torres, G., Andersen, J., and Gimenez, A. 2010, A & Ap Rv, 18, 67
- Udalski, A., and Evans, N. R. 1993, AJ, 106, 348
- Usenko, I. A., Kniazev, A. Y., Berdnikov, L. N., Fokin, A. B., and Kravtsov, V. V. 2014, AstL, 40, 435
- Wahhaj, Z. et al. 2015, A&A, 581A, 24
- Welch, D. L., Evans, N. R., Lyons, R. W., Harris, H. C., Barnes, T. G., Slovak, M. H. and Moffett, T. J. 1987, PASP, 99, 610.
- Wesselius, P. R., van Duinen, Aalders, J. W. G., and Kester, D. 1980, A&A, 85, 221